

Indoloquinoline derivatives as promising multi-functional anti-Alzheimer agents

Ashish M. Kanhed , Dushyant V. Patel , Nirav R. Patel , Anshuman Sinha , Priyanka S. Thakor , Kishan B. Patel , Navnit K. Prajapati , Kirti V. Patel & Mange Ram Yadav

To cite this article: Ashish M. Kanhed , Dushyant V. Patel , Nirav R. Patel , Anshuman Sinha , Priyanka S. Thakor , Kishan B. Patel , Navnit K. Prajapati , Kirti V. Patel & Mange Ram Yadav (2020): Indoloquinoline derivatives as promising multi-functional anti-Alzheimer agents, Journal of Biomolecular Structure and Dynamics, DOI: [10.1080/07391102.2020.1840441](https://doi.org/10.1080/07391102.2020.1840441)

To link to this article: <https://doi.org/10.1080/07391102.2020.1840441>

 View supplementary material 

 Published online: 28 Oct 2020.

 Submit your article to this journal 

 View related articles 

 View Crossmark data 



Indoloquinoline derivatives as promising multi-functional anti-Alzheimer agents

Ashish M. Kanhed^{a,b}, Dushyant V. Patel^a, Nirav R. Patel^a, Anshuman Sinha^a, Priyanka S. Thakor^a, Kishan B. Patel^a, Navnit K. Prajapati^a, Kirti V. Patel^a and Mange Ram Yadav^a

^aFaculty of Pharmacy, Kalabhavan Campus, The Maharaja Sayajirao University of Baroda, Vadodara, India; ^bShobhaben Pratapbhai Patel - School of Pharmacy & Technology Management, SVKMs NMIMS University, Mumbai, India

Communicated by Ramaswamy H. Sarma

ABSTRACT

To confront a disease like Alzheimer's disease having complex pathogenesis, development of multitarget-directed ligands has emerged as a promising drug discovery approach. In our endeavor towards the development of multitarget-directed ligands for Alzheimer's disease, a series of indoloquinoline derivatives were designed and synthesized. In vitro cholinesterase inhibition studies revealed that all the synthesized compounds exhibited moderate to good cholinesterase inhibitory activity. 6-(6-(Piperidin-1-yl)hexyl)-6*H*-indolo[2,3-*b*]quinoline **9f** was identified as the most potent and selective BuChE inhibitor ($IC_{50} = 0.96 \mu M$, selectivity index = 0.17) that possessed 2 fold higher BuChE inhibitory activity compared to the commercially approved reference drug donepezil ($IC_{50} = 1.87 \mu M$). Moreover, compound **9f** is also endowed with self-induced $A\beta_{1-42}$ aggregation inhibitory activity (51.24% inhibition at $50 \mu M$ concentration). Some of the compounds of the series also displayed moderate anti-oxidant activity. To perceive a putative binding mode of the compound **9f**, molecular docking studies were carried out, and the results pointed out significant interactions of compound **9f** with the enzymes in the binding sites of cholinesterases as well as $A\beta_{1-42}$. Additionally, compound **9f** exhibited favorable in silico ADMET properties. Put together these findings project compound **9f** as a potential multitarget-directed ligand in the direction of developing novel anti-AD drugs.

ARTICLE HISTORY

Received 15 July 2020
Accepted 18 October 2020

KEYWORDS

Alzheimer's disease; MTDL; cholinesterase inhibitor; anti- $A\beta$ aggregation; indoloquinoline

Introduction

Alzheimer's disease (AD), the most prominent type of dementia, is a progressive neurodegenerative disease prevalent amongst elderly people (Scheltens et al., 2016). Almost 50 million people are suffering from AD worldwide, and if no cure or preventive measures are discovered soon, the number will grow up significantly to 150 million by 2050 (Patterson, 2018). The etiology of AD is very intricate, various aspects like scarcity of acetylcholine (ACh) (Talesa, 2001), abnormal amyloid- β ($A\beta$) accumulation (Hardy & Higgins, 1992; Selkoe, 2003), tau hyperphosphorylation (Maccioni et al., 2010), oxidative stress (Bonda et al., 2010) and dyshomeostasis of biometals (Greenough et al., 2013) are hypothesized to play significant roles in the etiology of AD.

According to the cholinergic hypothesis, low levels of ACh in the brain is a crucial factor in the pathogenesis of AD (Talesa, 2001). Two types of cholinesterase enzymes (ChEs), namely, acetylcholinesterase (AChE) and butyrylcholinesterase (BuChE) are present in the central nervous system (CNS) that can quickly hydrolyze acetylcholine (ACh). Therefore, ChE inhibition remains an effective strategy to enhance ACh levels within the brain (Bartus et al., 1982). Both ChEs hydrolyze ACh, but BuChE is less substrate-specific than AChE, as

BuChE can also hydrolyze other molecules, for example, succinylcholine, adipoylcholine, benzoylcholine, and neurotoxic peptides (Lane et al., 2006; Pohanka, 2011). In a disease free brain, AChE mainly causes ACh hydrolysis but as the Alzheimer's advances, AChE level declines, and the BuChE level augments up to 40 to 90% in the temporal cortex and hippocampus areas of the brain (Hartmann et al., 2007). BuChE performs both neural as well as non-neural functioning roles. Also the clinical data has suggested the various roles of elevated levels of BuChE in AD, such as the aggregation of hyperphosphorylated tau protein and extracellular deposition of the $A\beta$ (Greig et al., 2002). Several ChE inhibitors like donepezil, tacrine, rivastigmine, and galantamine have been approved for the treatment of AD. These inhibitors, however, induce classical cholinergic side effects, such as digestive tract reactions and hepatotoxicity that severely affect their therapeutic goals. Therefore, the development of safe, effective and moderately selective BuChE inhibitors may present a novel approach for the treatment of AD patients of primary as well as late stages (Dighe et al., 2016; Greig et al., 2005).

Another significant hypothesis is amyloid hypothesis, which suggests the role of $A\beta$ plaques in the AD

pathogenesis (Hardy & Higgins, 1992; Selkoe, 2003). The amyloid precursor protein (APP) is hydrolyzed sequentially by α -, β - and γ -secretase enzymes to produce A β peptides that can aggregate into monomers, oligomers, and large A β plaques, and get deposited in the regions of hippocampal and basal ganglia of the patient's brain. These aggregates initiate pathogenic cascade of events and finally lead to neuronal loss and dementia (O'Brien & Wong, 2011). The A β plaques formed from A β_{1-42} are neurotoxic and continuously activate inflammatory factors, such as IL-6 and TNF- α . Moreover, because of self oxygen-free radical donation activity of A β_{1-42} , it directly activates reactive oxygen species (ROS) which subsequently affect the regular physiological functions of neurocytes (Cheignon et al., 2018). Hence, the A β_{1-42} aggregation prevention could serve as a coherent approach for the treatment of AD.

Recent research has emphasized that oxidative stress is one of the earliest events in AD pathogenesis. Inequity among the production and quenching of free radicals formed from oxygen species generates oxidative stress (Lobo et al., 2010). Through pathological redox steps, ROS and reactive nitrogen species (RNS) can denature biomolecules like lipids, proteins and nucleic acids and can cause serious damage to tissue by apoptosis and necrosis (Uttara et al., 2009). This suggests that oxidative stress also plays a crucial role in the pathogenesis of AD, causing neuronal dysfunction and cell death (Zhao & Zhao, 2013).

Considering the facts that ChE inhibition provides a symptomatic treatment to AD, increased levels of BuChE are observed in the AD patients' brains, A β aggregation and the ROS system play vital roles in neurodegeneration, in this report a series of indolo[2,3-*b*]quinoxaline derivatives were designed, synthesized, and tested for their multifactorial anti-AD activities, which includes cholinesterase and A β aggregation inhibitory activity along with promising antioxidant properties. The ADMET properties of the synthesized derivatives were predicted *in silico*. Molecular modeling studies were carried out to understand the binding modes of the derivatives with the target proteins.

Rationale of designing

The multifactorial nature of AD prompts treatment with multi-target-directing ligands (MTDLs) to tackle the important pathological hallmarks (Cavalli et al., 2008). Though ChEIs render only symptomatic and momentary benefits to the patients, they still are the preferred medicines. The oxidative stress and neurotoxic A β plaques perform important functions in the AD pathogenesis. However, A β aggregation inhibitors or antioxidants all alone might not be sufficient to resist a highly intricate pathological condition of AD. Thus focusing inhibition of multiple targets including cholinesterase and A β aggregation along with antioxidant activities might be a desirable pick to offset the progress of this multifaceted disease.

Some nitrogen-containing heterocycles, especially alkaloids, have been recognized as promising candidates in our quest for new drug leads for the treatment of AD. In particular, several indole alkaloids nitrarine **1a**, hirsutine **1b**, rauwolscine

1c, catharanthine **1d**, vallesiachotamine lactone **1e**, vallesiachotamine **1f**, faspaplysin **1g**, infractopicrin **1h**, angustine **1i**, prunifoleine **1j** and cryptolepine **1k** are reported to possess cholinesterase inhibitory activity (Figure 1) (Brunhofer et al., 2012). Recently, various ring-hybrids containing indole nucleus, e.g. triazinoindole hybrids (Patel et al., 2019, Patel et al., 2020), donepezil-chromone-melatonin hybrids (Pachon-Angona et al., 2019), tacrine – melatonin hybrids (Rodríguez-Franco et al., 2006), carbamate derivatives of indolines (Yanovsky et al., 2012) and melatonin-*N,N*-dibenzyl(*N*-methyl)-amine hybrids (López-Iglesias et al., 2014) have been reported as multifunctional agents for AD treatment suggesting indole ring as an important privileged scaffold for CNS-active agents which could augment the search for novel therapeutics for AD.

E Ramos *et al* reported new tacrine derivatives like quinoxalinetacrine (QT) hybrid QT78 for the treatment of AD (Figure 2). QT78 is less toxic but less potent than tacrine and showed selective BuChE inhibition (*hAChE*, IC₅₀ = 22.0 μ M; *hBuChE*, IC₅₀ = 6.79 μ M) (Ramos et al., 2019). The toxicity associated with tacrine and QT78 molecule might be due to their oxidative hydroxylation by CYP1A2 followed by rearrangement to the reactive quinonemethide intermediates. These metabolites have the potential to bind irreversibly to liver cells and lead to hepatic necrosis (McEneny-King et al., 2017). Replacing the 5,6,7,8-tetrahydroquinoline ring in QT78 with an indole ring could retard the rearrangement step in metabolism and the presence of indole ring additionally might provide a beneficial effect against the oxidative stress. A combination of these two privileged scaffolds, indole ring and the quinoxaline ring by molecular hybridization approach resulted in a tetracyclic indolo[2,3-*b*]quinoxaline scaffold (Figure 2). The planar aromatic structure of the indolo[2,3-*b*]quinoxaline scaffold has the potential to block the π -stacking in amyloid fibril formation and could inhibit self-induced A β_{1-42} aggregation.

The molecular interactions of the designed indolo[2,3-*b*]quinoxaline scaffold were assessed by performing the molecular docking of the scaffold within the binding sites of ChE enzymes. The indolo[2,3-*b*]quinoxaline scaffold demonstrated promising and stable binding affinities with both the AChE and BuChE enzymes (Figure 3). The indolo[2,3-*b*]quinoxaline scaffold showed very good stability within the active sites of the enzymes. In AChE, the ligand-receptor complex stability was observed mainly due to strong π - π interactions between the scaffold and Trp84 and Phe330 (*hAChE*: Trp86 and Tyr337) of the active site. Further, this complex was stabilized by hydrogen bonding with His440 (*hAChE*: His447), while the same molecule in the active binding site of BuChE showed promising π - π interactions with Trp82 along with a hydrogen bond with His438. In the *in vitro* enzyme inhibition assay, indolo[2,3-*b*]quinoxaline offered IC₅₀ values of 14.96 μ M against AChE and 13.26 μ M against BuChE. Based on this moderately promising activity of the designed indolo[2,3-*b*]quinoxaline scaffold, chemical modifications were carried out in it by including a range of alkyl/benzyl groups to come up with some potential leads and to frame a tangible SAR for the series. Accordingly, compounds of the two series (II, III), as shown in Figure 2, were synthesized and discussed here in this report.

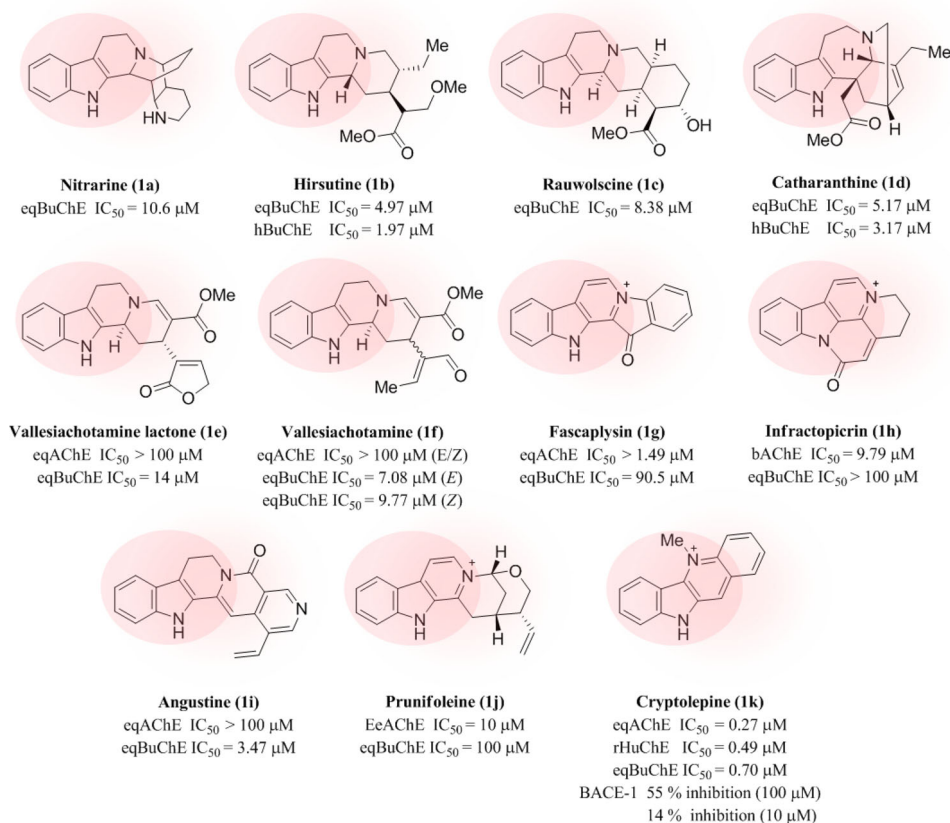


Figure 1. Some natural indole alkaloids reported in the literature for treatment of AD.

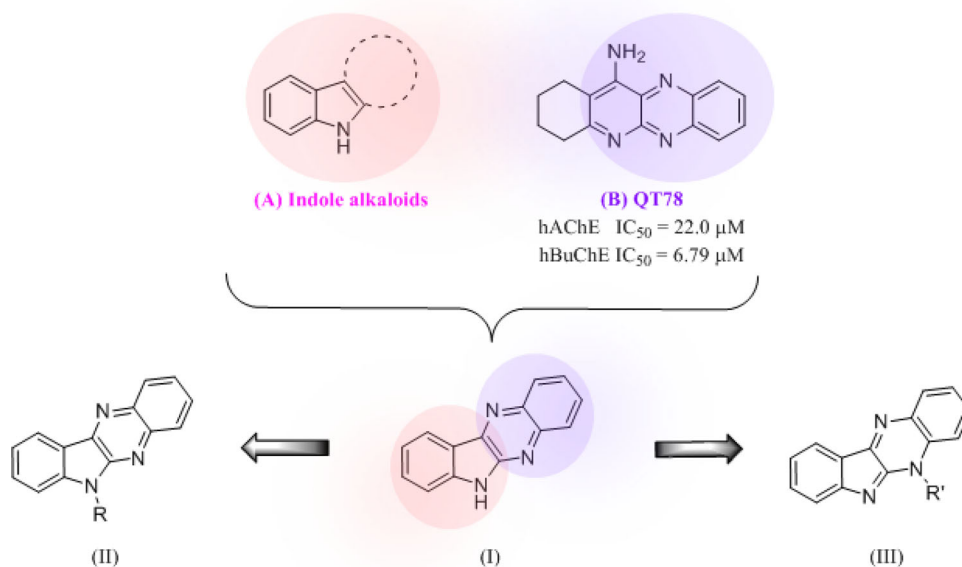


Figure 2. Design of indoloquinoline derivatives by molecular hybridization approach.

Results and discussion

Chemistry

Compounds **3a-3l** were synthesized as depicted in Scheme 1. *N*-substituted isatins **2b-2l** were prepared from commercially available isatin **2a** by nucleophilic substitution reaction with

different alkyl/benzyl halides. These isatin/*N*-substituted isatins were further condensed with 1,2-diaminobenzene in the presence of acetic acid under microwave conditions to yield the indolo[2,3-*b*]quinoxaline derivatives **3a-3l** (Avula et al., 2012).

5-Substituted indolo[2,3-*b*]quinoxaline derivatives **7a-7k** were synthesized as per the route depicted in the Scheme 2.

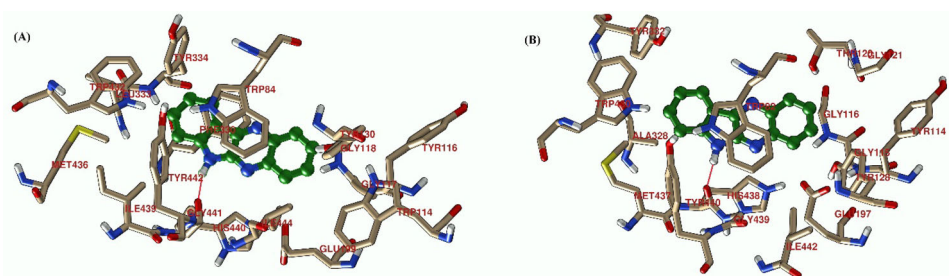
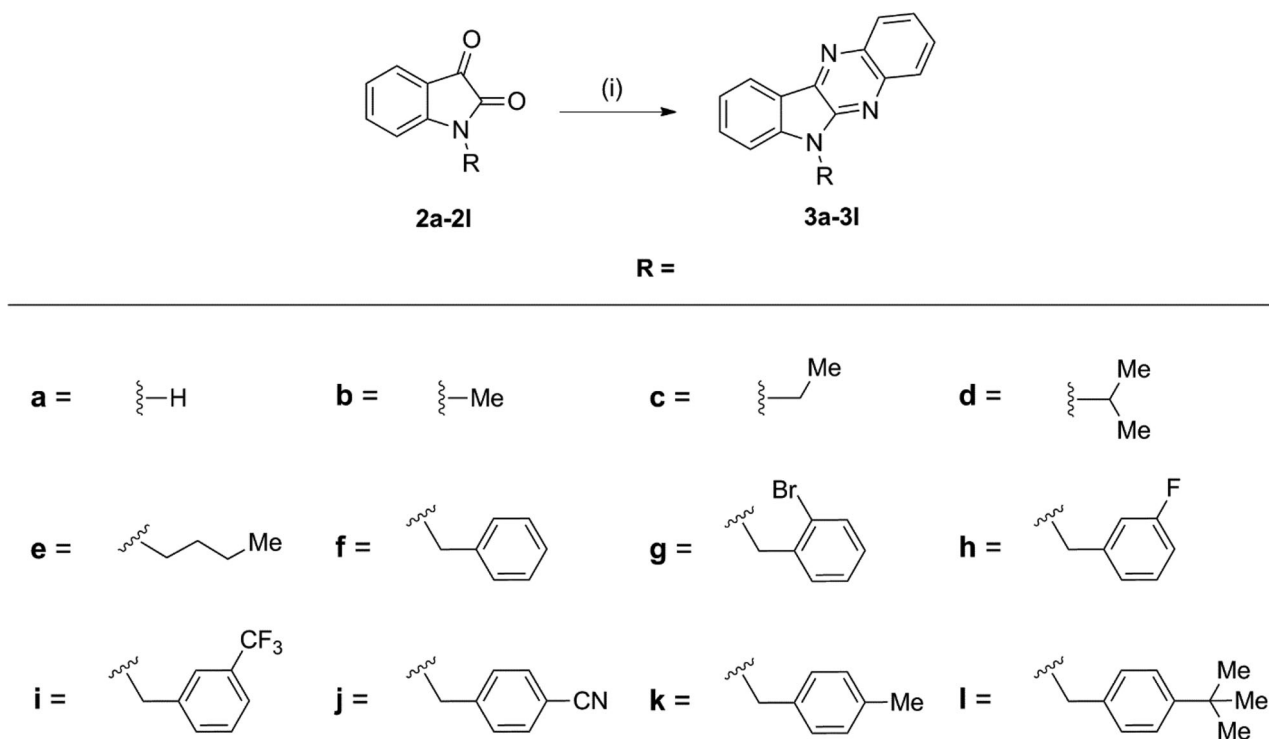


Figure 3. Molecular interaction of indolo[2,3-*b*]quinoxaline with (A) AChE and (B) BuChE.



Scheme 1. Synthesis of compounds **3a-3l**. Reagents and conditions: (i) 1,2-Diaminobenzene, AcOH, microwave 450 W, 8–10 min.

1-Fluoro-2-nitrobenzene **4** was treated with substituted benzyl/phenethylamines in the presence of potassium carbonate as the base in DMF to obtain the substituted *N*-benzyl/phenethyl-2-nitrophenylamines **5a-5k**. These nitro derivatives **5a-5k** were reduced by zinc/acetic acid to *N*₁-substituted 1,2-diamine intermediates **6a-6k** which were condensed with isatin **2a** as per the procedure adopted for compound **3a** to give the cyclized 5-substituted indolo[2,3-*b*]quinoxaline derivatives **7a-7k**.

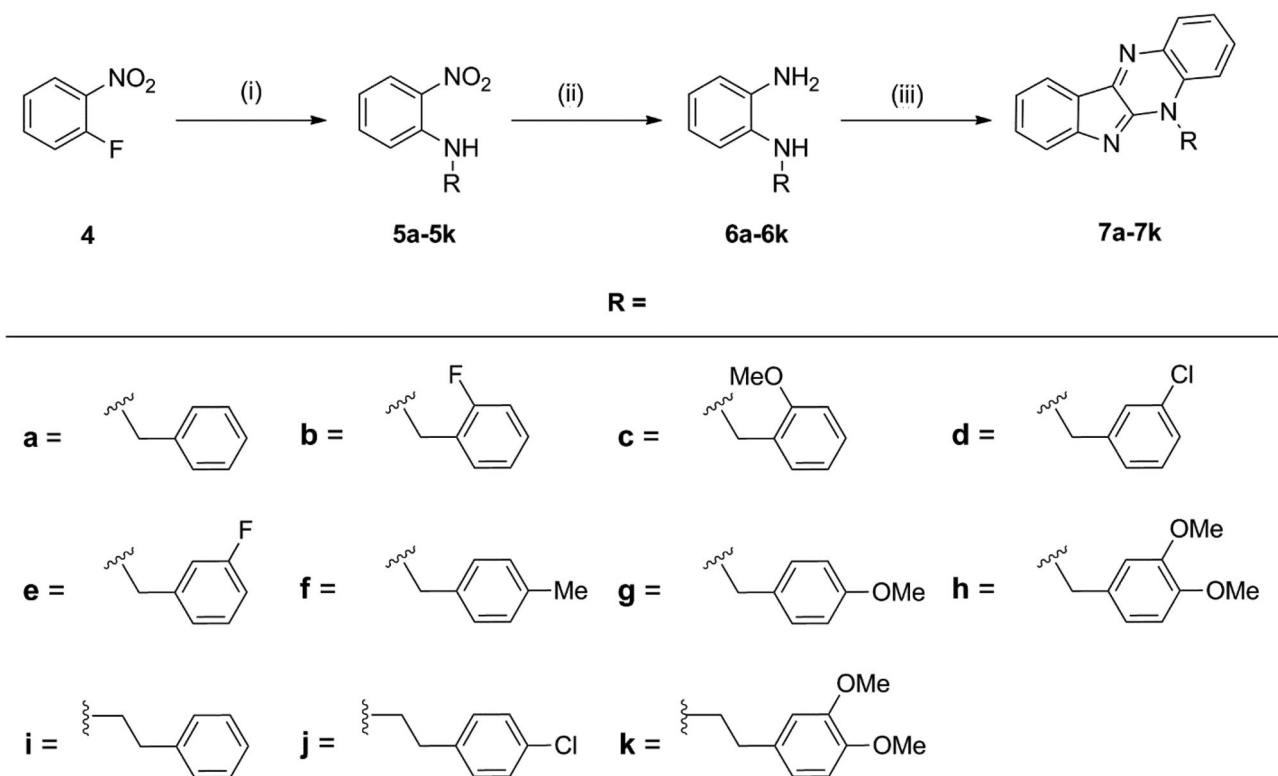
6-(Aminoalkyl)-6*H*-indolo[2,3-*b*]quinoxaline derivatives (**9a-9f**) and 1-(6-(6*H*-indolo[2,3-*b*]quinoxalin-6-yl)hexyl)alkylamides (**10a, 10b**) were synthesized as per the route showed in the Scheme 3. *N*-Bromoalkyl-6*H*-indolo[2,3-*b*]quinoxalines (**8a-8c**) were obtained from compound **3a** by reacting it with dibromoalkane in the presence of sodium hydroxide (Gu et al., 2017). Aminodebromination of compounds **8a-8c** by excess secondary amines in THF leads to 6-substituted aminoalkyl-6*H*-indolo[2,3-*b*]quinoxalines. To assess the importance of the basic alicyclic amine function in the structure, alicyclic amides were also prepared. Compounds **10a** and **10b** were synthesized by the reaction of pyrrolidinone and piperidinone with **8c** in the presence of sodium hydride.

Biological evaluation

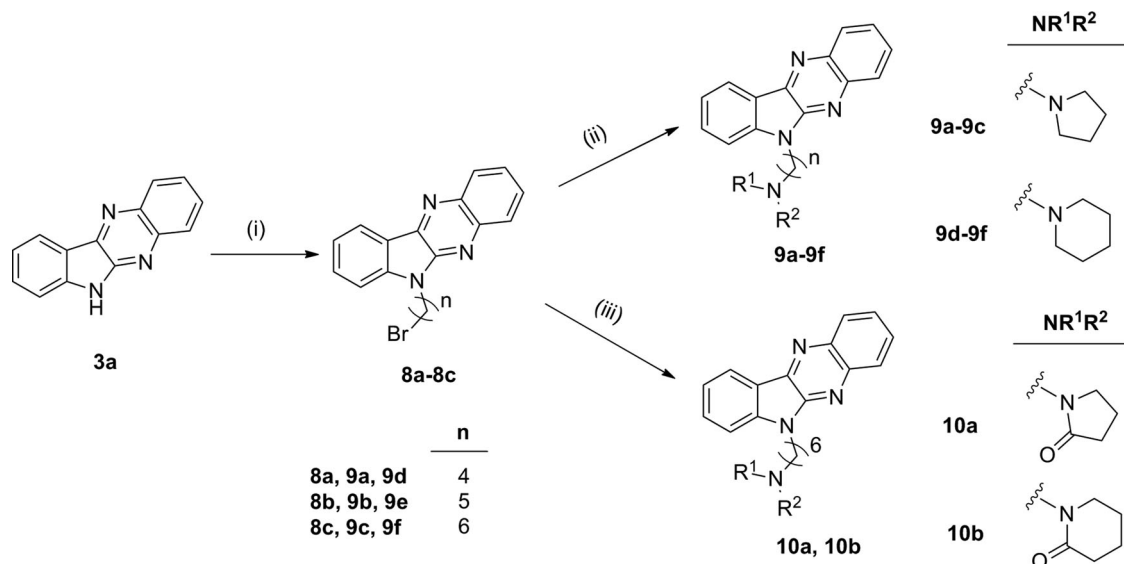
Inhibition studies on AChE and BuChE

The anti-cholinesterases (anti-ChE) activity of synthesized compounds were assessed *in vitro* using the Ellman's assay, as previously reported by our group (Kanhed et al., 2015; Patel et al., 2019, Patel et al., 2020; Shidore et al., 2016 Sinha et al., 2015). Tacrine and donepezil were used as standard reference drugs for this study. The IC₅₀ values determined for the compounds against both the enzymes along with their selectivity indices (SI) are summarized in Tables 1 and 2. As shown in Table 1 compound **3a** showed considerable inhibitory activity (AChE, IC₅₀ = 14.96 μM; BuChE, IC₅₀ = 13.26 μM). This encouraging finding of the lead **3a** provoked us to look at different substituents on the indole and quinoxaline ring nitrogen to frame a considerable structure-activity relationship.

The alkyl substituents introduction on indole as in compounds **3b-3e** showed decrease in activity. Among them, compound **3b** with the methyl group showed comparable inhibition activity (AChE, IC₅₀ = 13.37 μM; BuChE, IC₅₀ = 15.80 μM) to the parent compound **3a**. Incorporation of



Scheme 2. Synthesis of compounds **7a-7k**. Reagents and conditions: (i) RNH_2 , K_2CO_3 , DMF, 60°C ; (ii) Zn, AcOH, MeOH, rt, 6–8 hrs; (iii) Isatin (**2a**), AcOH, microwave 450 W, 8–10 min.



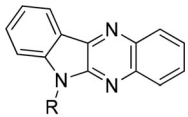
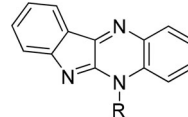
Scheme 3. Synthesis of compounds **9a-9f**, **10a** and **10b**. Reagents and conditions: (i) $\text{Br}(\text{CH}_2)_n\text{Br}$, NaOH, THF, reflux; (ii) $\text{R}^1\text{R}^2\text{NH}$, THF, reflux; (iii) $\text{R}^1\text{R}^2\text{NH}$, NaH, THF.

benzyl and substituted benzyis at indole-NH exhibited reduced inhibitory activity. So as compared to compound **3a**, the presence of simple alkyls/substituted benzyis on indole-NH ring did not show any significant improvement in activity. Introducing alkyl substituents on the nitrogen of the quinoxaline ring as in compounds **7a-7k** exhibited a mixed effect on the inhibitory activity of the compounds. As mentioned in Table 1, all the compounds **7a-7k** showed IC_{50} in the range of 9–17 μM for AChE and 13–30 μM for BuChE. Amongst them, compound **7h** having 3,4-dimethoxybenzyl side chain showed better AChE inhibitory activity as

compared to the lead molecule, whereas BuChE activity remained the same as that of compound **3a**.

When the *N*-butyl moiety in compound **3e** was replaced with 4-(1-pyrrolidinyl)butyl (compound **9a**) and 4-(1-piperidinyl)butyl (compound **9d**) moieties, considerable raise in inhibitory activities against both the enzymes observed, particularly BuChE inhibitory activity got increased notably. Compounds **9a** and **9d** exhibited inhibitory activities (AChE; $\text{IC}_{50} = 14.39 \mu\text{M}$, $11.53 \mu\text{M}$, respectively) and (BuChE; $\text{IC}_{50} = 4.48 \mu\text{M}$, $2.56 \mu\text{M}$, respectively). Joining of the tetracyclic indoloquinoline moiety with cyclic amines like pyrrolidine

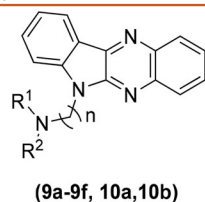
Table 1. *In Vitro* Inhibition activity and Selectivity Index (SI) of Compounds 3a-3l, 7a-7k against AChE and BuChE.

 (3a-3l)					 (7a-7k)				
Compd	R	IC ₅₀ ± SEM (μM)			Compd	R	IC ₅₀ ± SEM (μM)		
		AChE ^a	BuChE ^b	SI ^c			AChE ^a	BuChE ^b	SI ^c
3a		14.96 ± 0.71	13.26 ± 1.05	0.89	7a		14.78 ± 0.19	16.79 ± 0.22	1.14
3b		13.37 ± 1.18	15.80 ± 1.22	1.18	7b		12.07 ± 0.15	21.66 ± 0.18	1.79
3c		17.47 ± 0.78	22.29 ± 1.19	1.28	7c		13.70 ± 0.18	24.95 ± 0.26	1.82
3d		19.14 ± 1.51	18.56 ± 0.45	0.97	7d		16.88 ± 0.26	30.01 ± 0.22	1.78
3e		19.98 ± 0.35	21.01 ± 0.53	1.05	7e		16.39 ± 0.21	15.01 ± 0.25	0.92
3f		24.09 ± 1.16	13.99 ± 1.21	0.58	7f		15.81 ± 0.14	32.21 ± 0.28	2.04
3g		20.28 ± 0.84	35.99 ± 1.18	1.77	7g		12.18 ± 0.15	25.27 ± 0.17	2.07
3h		20.92 ± 1.09	16.15 ± 0.56	0.77	7h		9.42 ± 0.54	13.50 ± 0.61	1.43
3i		26.63 ± 1.23	93.48 ± 2.53	3.51	7i		13.07 ± 0.78	20.47 ± 0.89	1.57
3j		20.59 ± 1.28	24.88 ± 1.16	1.21	7j		17.38 ± 1.22	21.74 ± 1.74	1.25
3k		24.19 ± 1.76	33.12 ± 1.52	1.37	7k		13.75 ± 0.71	18.90 ± 0.24	1.37
3l		19.08 ± 1.08	11.95 ± 0.85	0.63					

^aAChE from human erythrocytes; IC₅₀, 50% inhibitory concentration (means ± SEM of three experiments).^bBuChE from equine serum.^cSelectivity index = IC₅₀ (BuChE)/IC₅₀ (AChE).

and piperidine through four carbon atom spacers enhanced BuChE inhibition significantly in comparison to that of simple alkyl/benzyl substituted indoloquinoline derivatives. On the basis of this finding, it was decided to evaluate the requirement of the attached basic amine and effect of the linker length on the cholinesterase inhibition activity of resulting compounds. As mentioned in Table 2, all the compounds **9a-9f** showed promising inhibitory activity against both ChE enzymes, IC₅₀ values ranging from 0.96 to 2.56 μM for BuChE and from 5.80 to 11.53 μM for AChE. These observations recommended the presence of alicyclic amines is necessary requirement for the ChE inhibitory activity as all the compounds bearing pyrrolidino and piperidino moieties exhibited strong ChE inhibition.

Change in the length of carbon chain showed alteration in inhibitory activity. A comparative analysis of the inhibitory potential of compounds **9d**, **9e** and **9f** carrying a piperidino ring, revealed that compound **9f** (*n* = 6, IC₅₀ value of 0.96 μM) showed the highest BuChE inhibitory activity whereas, the compound **9d** (*n* = 4, IC₅₀ value of 2.56 μM) and compound **9e** (*n* = 5, IC₅₀ value of 1.40 μM) exhibited 2.6-fold and 1.5-fold less BuChE inhibitory activities in comparison to compound **9f** (Table 2). Similar type of pattern was also found for the compounds **9a**, **9b** and **9c**. The inhibitory potential of compounds **9a**, **9b** and **9c** having a pyrrolidino ring, revealed that compound **9c** (*n* = 6, IC₅₀ value of 1.07 μM) exhibited the highest BuChE inhibitory activity while compound **9a** (*n* = 4, IC₅₀ value of 4.48 μM) and compound **9b** (*n* = 5, IC₅₀ value of 1.70 μM)

Table 2. *In Vitro* Inhibition activity and Selectivity Index (SI) of Compounds 9a-9f, 10a and 10b against AChE and BuChE.

Compd	n	R ¹ R ² N	IC ₅₀ ± SEM (μM)		SI ^c	Aβ ₁₋₄₂ aggregation Inhibition (%)		RP of DPPH IC ₅₀ ± SEM (μM) or (% inhibition at 100 μM) ^d
			AChE ^a	BuChE ^b		25 μM	50 μM	
9a	4		14.39 ± 1.12	4.48 ± 0.22	0.31	17.25 ± 0.31	41.37 ± 0.75	144.88 ± 3.12
9b	5		10.31 ± 0.43	1.70 ± 0.27	0.16	14.63 ± 0.64	38.72 ± 0.28	168.43 ± 4.56
9c	6		6.2 ± 0.41	1.07 ± 0.51	0.18	21.37 ± 0.28	49.77 ± 0.46	146.19 ± 2.12
9d	4		11.53 ± 0.76	2.56 ± 0.23	0.22	18.98 ± 0.15	42.39 ± 0.44	155.81 ± 4.56
9e	5		7.27 ± 0.58	1.40 ± 0.70	0.19	18.35 ± 0.33	40.32 ± 0.28	132.37 ± 3.12
9f	6		5.80 ± 0.70	0.96 ± 0.31	0.17	26.40 ± 0.54	51.24 ± 0.55	134.43 ± 3.12
10a	6		6.63 ± 0.54	4.48 ± 0.15	0.68	17.58 ± 0.42	39.43 ± 0.74	> 500 (3.59 %)
10b	6		5.99 ± 0.37	5.01 ± 1.02	0.84	21.55 ± 0.62	46.32 ± 0.82	> 500 (3.17 %)
Tacrine			0.056 ± 0.01	0.008 ± 0.00	0.14	nd	nd	> 500 (17.2 %)
Donepezil			0.023 ± 0.01	1.87 ± 0.08	81.3	nd	nd	> 500 (5.41 %)
Curcumin			nd	nd	–	20.43 ± 0.72 μM (IC ₅₀)		nd
Ascorbic acid			nd	nd	–	nd	nd	13.91 ± 1.33 (95.43 %)

^aAChE from human erythrocytes; IC₅₀, 50% inhibitory concentration (means ± SEM of three experiments).

^bBuChE from equine serum.

^cSelectivity index = IC₅₀ (BuChE)/IC₅₀ (AChE).

^dRP of DPPH (%) = reduction percentage of DPPH.

showed 4.2-fold and 1.6-fold less BuChE inhibitory activities in comparison to compound **9c** (Table 2).

However, the inhibitory activity of these compounds against AChE was slightly lesser than that against BuChE, this could be because of structural and conformational variation among both the enzymes. Compound **9f** ($n=6$, IC₅₀ value of 5.80 μM) showed an acceptable level of AChE inhibition whereas compound **9d** ($n=4$, IC₅₀ value of 11.53 μM) and compound **9e** ($n=5$, IC₅₀ value of 7.27 μM) exhibited 1.9-fold and 1.2-fold less AChE inhibitory activities compared to compound **9f**. Compound **9c** ($n=6$, IC₅₀ value of 6.2 μM) exhibited an acceptable level of AChE inhibitory activity while compound **9a** ($n=4$, IC₅₀ value of 14.39 μM) and compound **9b** ($n=4$, IC₅₀ value of 10.31 μM) showed 2.3-fold and 1.7-fold less AChE inhibitory activities compared to compound **9c**. Piperidino moiety appeared to be a better choice over pyrrolidino moiety, as compounds **9d-9f** bearing piperidino moiety exhibited higher activity than the compounds **9a-9c** bearing pyrrolidino moiety as attachments.

When the amino functions in compounds **9c** and **9f** were replaced with the corresponding cyclic amide moieties, the BuChE inhibitory activity got notably diminished. Compound **10a** having pyrrolidinone moiety (IC₅₀ value of 4.48 μM) and compound **10b** having piperidinone moiety (IC₅₀ value of 5.01 μM) showed 4.2-fold and 5.2-fold less BuChE inhibitory activities compared to compounds **9c** and **9f**, respectively. However, the AChE inhibitory activity of the compounds **10a** and **10b** remained almost unaltered in comparison to the corresponding amine derivatives **9c** and **9f**. Similar to tacrine (SI value of 0.14), compounds **9c** (SI value of 0.18) and **9f** (SI value of 0.17) have shown higher selectivity for BuChE over AChE than donepezil (SI value of 81.3).

Self-mediated Aβ₁₋₄₂ aggregation inhibition study

The Aβ peptides forming amyloid plaques are product of APP due to cleavage mainly by β- and γ-secretases. Aβ

Table 3. Permeability (P_e 10^{-6} cm s^{-1}) of selected commercial drugs for the validation of the PAMPA-BBB permeation assay.

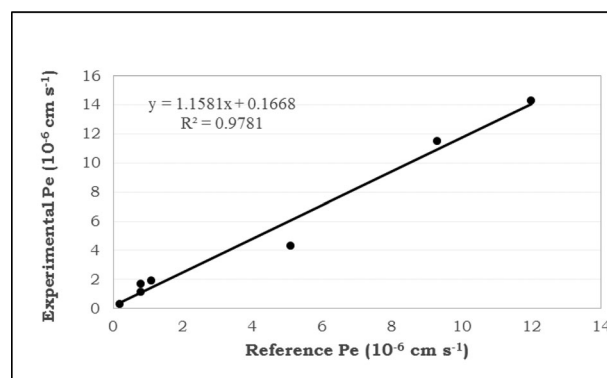
Sr. No.	Commercial drugs	$(P_e$ 10^{-6} cm $s^{-1})$	
		Reference value ^a	Experimental value
1	Dopamine	0.2	0.3 ± 0.1
2	Atenolol	0.8	1.1 ± 0.3
3	Ofloxacin	0.8	1.7 ± 0.5
4	Lomefloxacin	1.1	1.9 ± 0.3
5	Corticosterone	5.1	4.3 ± 0.6
6	Progesterone	9.3	11.5 ± 1.2
7	Donepezil	12.0	14.3 ± 1.7

^aTaken from reference (Di et al., 2003, Di et al., 2009). Data are expressed as mean ± SEM of three independent experiments.

with 40 and 42 units are the main forms present in the plaques. Though $A\beta_{1-40}$ is the predominant product in the proteolytic cleavage, we chose $A\beta_{1-42}$ to study the inhibition of compounds as it is more fibrillogenic in nature (Lane et al., 2018). Thioflavin T (ThT) fluorescence assay was used to understand the potency of the compounds to prevent self-mediated $A\beta_{1-42}$ aggregation (Li et al., 2013). Compounds having IC_{50} values (BuChE) less than 5 μ M were considered for this study. Here as positive control Curcumin was used in the assay and the compounds were tested at 25 μ M and 50 μ M concentrations and listed in Table 2. All these compounds exhibited moderate $A\beta_{1-42}$ aggregation inhibition ranging from 14.63 to 26.40% at 25 μ M concentration and 38.72–51.24% at 50 μ M concentration. Compound **9f** showed 26.40% (at 25 μ M concentration) and 51.24% (at 50 μ M concentration) inhibition of $A\beta_{1-42}$ aggregation. These anti- $A\beta$ aggregatory activities could be due to the presence of planar aromatic tetracyclic indoloquinoline ring in their structures.

Antioxidant activity [1,1-Diphenyl-2-picrylhydrazyl (DPPH) radical scavenging activity]

To evaluate the antioxidant or free radical scavenging potency of compounds, the DPPH radical scavenging assay is common and reliable method. Being a stable free radical, DPPH can accept an electron or hydrogen radical to become a stable molecule. On the basis of the ability of compounds under study to reduce DPPH-radical (purple color) to DPPHH (yellow) and the corresponding radical-scavenging potential were evaluated by a fall in the absorbance level at 517 nm (Patel et al., 2019, Patel et al., 2020). Compounds with IC_{50} (BuChE) less than 5 μ M were considered here for this study. Ascorbic acid was used as the positive control in this assay. All the test compounds showed moderate free radical scavenging activity with their IC_{50} values ranging from 132 μ M to 168 μ M (Table 2). Compounds **9e** and **9f** also showed moderate free radical scavenging activity (IC_{50} values 132.37 μ M and 134.43 μ M, respectively) compared to ascorbic acid (95.43% inhibition at 100 μ M concentrations), whereas tacrine and donepezil (IC_{50} values > 500 μ M) were found to be almost devoid of any free radical scavenging activity at these concentrations.

**Figure 4.** Linear correlation between experimental and reference permeabilities of selected commercial drugs using PAMPA-BBB assay. P_e (exp.) = 1.16 P_e (ref.) + 0.1668 ($R^2 = 0.9781$).**Table 4.** Permeability range (P_e 10^{-6} cm s^{-1}) of PAMPA-BBB assay.

	PBS:ethanol (70:30)
Compounds of low BBB permeation (CNS-)	$2.5 > P_e$
Compounds of uncertain BBB permeation (CNS+/-)	$4.8 > P_e > 2.5$
Compounds of high BBB permeation (CNS+)	$P_e > 4.8$

Table 5. Permeability (P_e 10^{-6} cm s^{-1}) of compound **9f** in the PAMPA-BBB permeation assay with its predicted penetration into the CNS.

Compd.	$(P_e$ 10^{-6} cm $s^{-1})$	Prediction
9f	16.2 ± 2.4	CNS+
Donepezil	14.3 ± 1.7	CNS+

Data expressed as mean ± SEM of three independent experiments.

In vitro blood-brain barrier (BBB) permeation assay

The permeability through BBB is a key parameter for the evaluation of novel CNS active molecules. The potential of indoloquinoline derivatives to penetrate the BBB was studied using a parallel artificial membrane permeation assay (PAMPA) (Di et al., 2003, Di et al., 2009). This assay is used for the prediction of passive diffusion of a molecule through BBB. The BBB permeability (P_e) of the most active compound **9f** was determined through a porcine brain lipid. The experimental permeability values [P_e (exp)] of seven commercial drugs with the reported permeability values [P_e (ref)] (Table 3) were compared for validation of the protocol, indicating a linear relationship i.e. P_e (exp) = 1.16 P_e (ref) + 0.1668 ($R^2 = 0.9781$) (Figure 4). From this equation and considering the limits for BBB permeation established by Di et al. (2003), it was reckoned that the compounds with P_e (exp) greater than 4.8×10^{-6} cm s^{-1} (Table 4) would be able to cross the BBB. Compound **9f** exhibited permeability value above this limit (Table 5). Therefore, P_e (exp) value propounded a high potential of the compound **9f** to cross the BBB by passive diffusion.

Computational studies

Molecular docking studies of compound **9f** and **9c** with ChEs

To comprehend the interactions and binding mode of the most active compound **9f** with the ChEs, docking studies

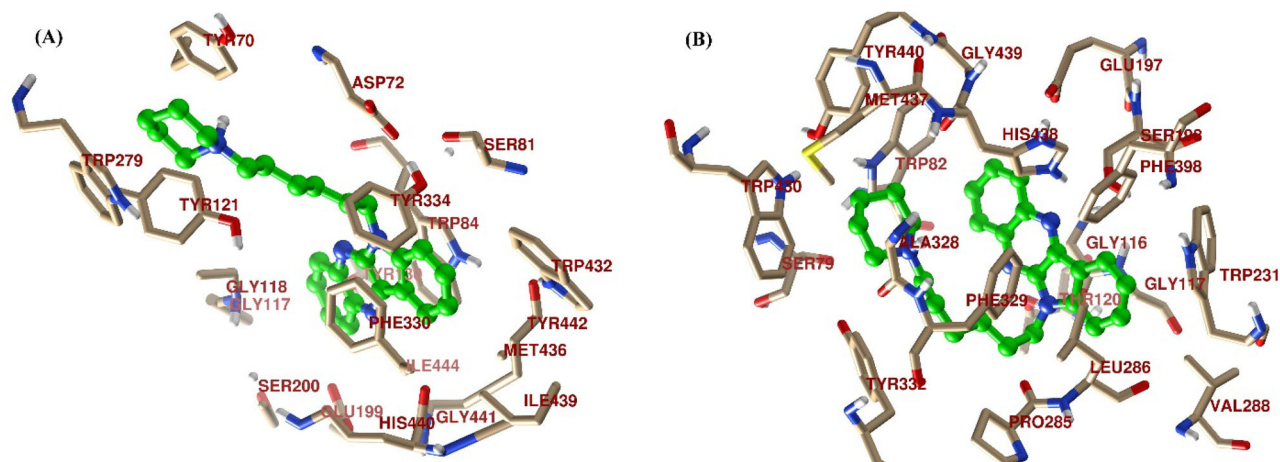


Figure 5. Docking interactions of **9f** with (A) AChE and (B) BuChE.

were carried out with the active sites of *Torpedo californica* AChE (*TcAChE*) (PDB code: 2CKM) and human BuChE (*hBuChE*) (PDB code: 4BDS). The validation of the developed grids for docking in Schrodinger suit was carried out by knocking out the existing co-crystallized ligands and re-docking the same ligands drawn afresh and energy minimized, using the prepared grids. In this re-performance study, very identical interactions to that of original co-crystallized ligands were observed between the enzymes and the re-docked ligands. In this re-docking study the root-mean-square deviation (RMSD) values of the redocked ligands in comparison to the original cocrystallized forms in the active site of 2CKM and 4BDS were found to be 0.40 and 0.26 Å, respectively.

To understand the molecular interactions of **9f** with AChE, *TcAChE* (PDB code: 2CKM) was retrieved from RCSB and humanized with *hAChE* to identify the sequence of amino acids from human interacting with compound **9f**. In the docking study of compound **9f** with AChE (Figure 5), the aromatic indolo[2,3-*b*]quinoxaline ring was observed to be stabilized comfortably in the active site of the enzyme by forming π - π interactions with Trp84 and Phe330 (*hAChE*: Trp86 and Tyr337). Due to the presence of six methylene linker, the piperidine ring of compound **9f** was observed to be oriented well towards the PAS. At physiological pH, the nitrogen of this ring could be protonated and showed highly stable pi-cation interaction with Trp279 (*hAChE*: Trp284) which conferred additional stability to the complex. In the docking study of compound **9c** with AChE, it was observed that the nitrogen of the pyrrolidine ring formed a weak hydrogen bond with Tyr121 (*hAChE*: Tyr124) and also part of the pyrrolidine ring was observed to be exposed to the solvent front and oriented differently. Due to these conformational differences, compound **9c** having pyrrolidine moiety possibly showed less AChE inhibitory activity than compound **9f**.

In the docking study of compound **9f** with BuChE (Figure 5), the terminal aromatic rings of indolo[2,3-*b*]quinoxaline exhibited π - π interactions with Trp82 and Trp231. Further, the nitrogen of the quinoxaline ring formed a stable hydrogen bond with His438. The pi-cation interaction between the nitrogen of the piperidine ring and Phe329 imparted additional stability to the ligand-receptor complex. Additionally, the piperidine ring was surrounded by the nonpolar/

hydrophobic residues comprising of Ala328, Phe329, Trp430 and Met434. While in the docking study of compound **9c** with BuChE, it was observed that the pyrrolidine ring didn't cause any promising interactions within the active site of the enzyme. Furthermore, part of the ring was observed to be oriented in the polar region of Ser79 and nonpolar aliphatic amino acid Gly78. These conformational differences could have made compound **9f** more active against BuChE than compound **9c**.

Molecular docking studies of compound **9f** with $A\beta_{1-42}$

To understand the binding interaction of compound **9f** with $A\beta_{1-42}$, docking study was performed using the X-ray crystal structure of human $A\beta_{1-42}$ (PDB code: 1IYT). As the active site or specific binding site is not precisely known, a blind docking study was performed using AutoDock 4.2. In blind docking, the ligand under study is allowed to freely move over the entire sequence of the protein and possible interactions are checked. In this study, the most stable ligand-receptor complex showed promising interactions (Figure 6). The aromatic indole ring exhibited π - π interaction with Phe19, whereas the quinoxaline ring formed strong pi-cation interaction with Lys16. Further, the protonated piperidine ring showed promising interaction by forming salt bridge as well as hydrogen bond with Glu11. These stacking and other non-covalent interactions could be responsible for the prevention of aggregation and deposition of insoluble $A\beta_{1-42}$ plaques and further events.

Molecular dynamics simulation studies

From the docking studies and biological evaluations, compound **9f** was observed as promising inhibitor. In order to validate, and know the time-dependent stability of the identified most potent compound **9f** with the AChE and BuChE receptor, a molecular dynamics study was carried out for the period of 10 ns. In order to understand the binding stability of the ligand receptor complex during the period of simulation time, statistical properties like RMSD-P, RMSF-P, and RMSD-L (P=protein; L=ligand), Van der Waals and

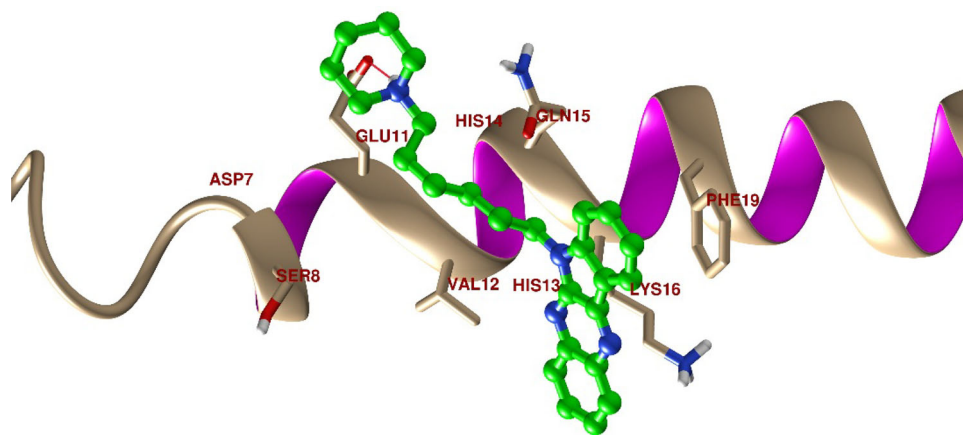


Figure 6. Docking interactions of compound **9f** with $A\beta_{1-42}$ (PDB code 1IYT). The possible hydrogen bonding between compound **9f** and Glu11 residue is shown by the red line.

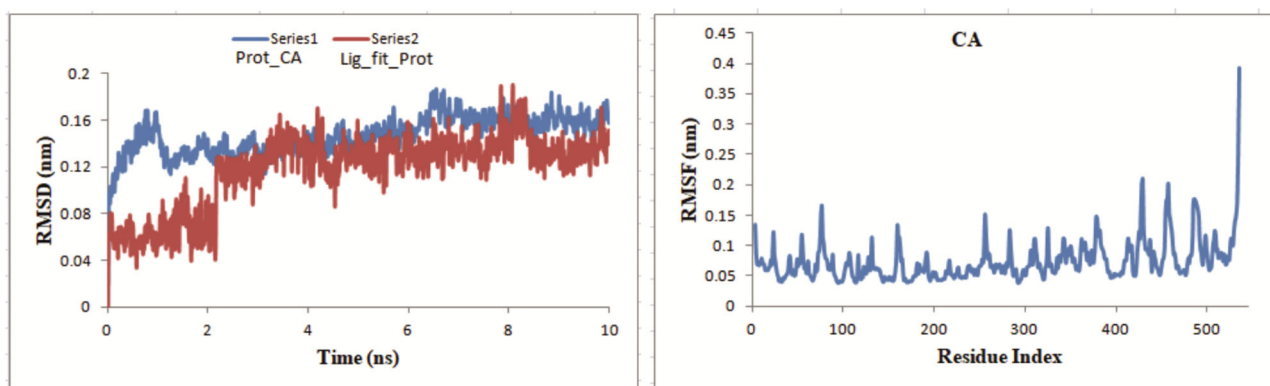


Figure 7. RMSD and RMSF plot for AChE with compound **9f**.

electrostatic interaction energies were examined to cross-check and support the stability of interactions. To calculate all these parameters, the original pose of the ligand-receptor complex was used as the reference frame.

The RMSD-P is fundamentally calculated to comprehend the extent of movements of different atoms or groups in the receptor in presence of ligand in the binding site of the receptor. Over the period of time, this explains the structural deviations and conformations of the receptor. For AChE in ligand-receptor complex the protein RMSD was observed in the range of 0.08 to 0.18 nm, and the average RMSD was 0.15 nm. Whereas the RMSD for ligand in contact with the residues of receptor active site was observed in the range of 0.04 to 0.18 nm with an average RMSD of 0.12 nm. Here, despite of having more rotatable bonds in the ligand structure, the RMSD value is found in the acceptable range, this strongly suggests that the compound **9f** is quite stable in the active site of receptor and not diffused from the binding site throughout the simulation period. The residual mobility and structural integrity of the receptor were enumerated with the help of RMSF. Including loop and terminal residues of the receptor, all the residues while having the compound **9f** in the active site, showed the RMSF below 0.4 nm (Figure 7). Further, the short-range electrostatic (Coul-SR) and *van der Waal*/hydrophobic (LJ-SR) interaction energies between the ligand and the receptor were calculated within Gromacs.

The average of -12.41 ± 2.6 kJ/mol (Coul-SR) and -212.54 ± 2.6 kJ/mol (LJ-SR) were observed. These observations suggested that the ligand interacted promisingly with the receptor active site by the contribution of both hydrophobic and electrostatic interactions; wherein the role of hydrophobic interactions was observed to be higher than that of electrostatic interactions throughout the simulation period.

Similarly, the MD study of compound **9f** with the BuChE receptor was also carried out. Wherein the average protein RMSD for BuChE was found to be 0.14 nm while for the ligand in contact with the protein it was 0.11 nm indicating that was stable in the active site and did not diffuse out of it during the complete simulation period. Here the RMSF for all the residues was found below 0.2 nm (Figure 8).

The average of -41.88 ± 0.65 kJ/mol (Coul-SR) and -179.11 ± 0.61 kJ/mol (LJ-SR) were observed suggesting that the role of hydrophobic interaction is more than electrostatic interaction in ligand-receptor stability.

In silico prediction of physicochemical and pharmacokinetics parameters

Approximately 40% of drug candidates abort in the clinical trials due to unacceptable ADME (absorption, distribution, metabolism, and excretion) profile. These late-stage dead ducks impart a massive hike in the cost of development of a

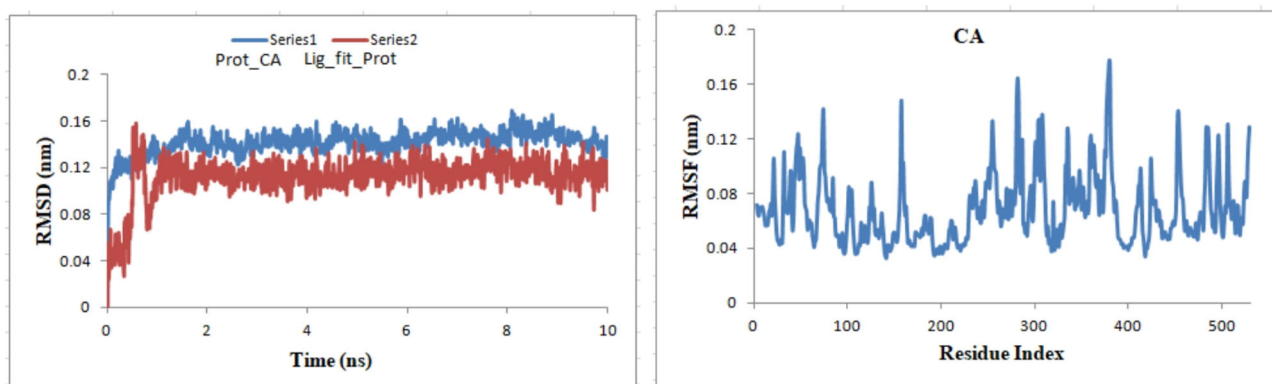


Figure 8. RMSD and RMSF plot for BuChE with compound 9f.

Table 6. *In-silico* calculated ADME properties of 9c, 9f, Tacrine and Donepezil^a.

Properties	Limit	9c	9f	Donepezil	Tacrine
MW	130–725	372.521	386.539	379.498	198.267
HBD	0–6	0	0	0	1.5
HBA	2–20	4	4	5.5	2
QLogP _{o/w}	–2 to 6.5	5.64	5.947	4.242	2.536
Rule of Five violation	0–1	1	1	0	0
NRB	0–8	7	7	6	1
PSA	7 to 200	32.268	31.315	46.234	33.825
SASA	300 to 1000	749.37	769.868	681.675	425.06
Volume	500–2000	1316.084	1359.562	1248.451	701.299
QPPCaco	–	1387.038	1487.168	1070.771	2965.755
% HOA	–	100	100	100	100
QPPMDCK	–	779.49	840.486	589.289	1602.036
QLogBB	–3 to 1.2	0.247	0.279	0.223	0.047
CNS	–	1	1	1	1
QLogKhSa	–1.5 to 1.5	1.071	1.198	0.516	0.049
QLogS	–6.5 to 0.5	–5.964	–6.353	–4.059	–3.036
#rtvFG	–	0	0	0	0
#star	–	0	0	0	0

^aMW: molecular weight, HBD: hydrogen-bond donor atoms, HBA: hydrogen-bond acceptor atoms, QLogP_{o/w}: Predicted octanol/water partition coefficient, NRB: number of rotatable bonds, PSA: polar surface area, SASA: total solvent accessible surface area, QPPCaco: Caco-2 cell permeability in nm/s, % HOA: human oral absorption on 0–100% scale, QLogBB: brain/blood partition coefficient, QPPMDCK: Predicted apparent MDCK cell permeability in nm/s, CNS: predicted central nervous system activity on a –2 (inactive) to +2 (active) scale, QLogKhSa: binding to human serum albumin, QLogS: predicted aqueous solubility, #rtvFG: number of reactive functional groups; #star: number of parameters with values that fall outside the 95% range of similar values for known drugs.

new drug. Hence, we planned to check virtual ADME parameters to affirm acceptable ADME performance during clinical trials. The *in silico* calculation of the ADME properties becomes comparatively simple and trustworthy because of significant advancements made in the computational science field. For the most active compounds **9c** and **9f**, the virtual physicochemical and pharmacokinetic parameters like Lipinski's parameters, NRB, PSA, QPPCaco, QLogBB, QPPMDCK, QLogKhSa were calculated using QikProp module (Table 6) (QikProp, 2018).

Lipinski's rule of five suggests that most "drug-like" molecules contain $\log P \leq 5$, hydrogen bond donors ≤ 5 , hydrogen bond acceptors ≤ 10 and molecular weight ≤ 500 (Lipinski et al., 1997). This rule explains the reason for various physico-chemical behavior of drug-like molecules, such as poor absorption or permeation occurs mainly when drug-like molecules deviate from more than one Lipinski's rule. Compounds **9c** and **9f** violate only one limit of the Lipinski's rule of five, making them promising leads for further drug development. Veber and co-worker introduced two key parameters namely, the number of rotatable bonds (NRB)

and the topological Polar Surface Area (TPSA) (Veber et al., 2002). NRB which explains the molecular flexibility, is also a very promising descriptor explaining the drug oral bioavailability. For the better oral bioavailability, a molecule could have 0–8 number of rotatable bonds or less than 7 linear chains outside the rings. TPSA is another important descriptor that compared well with passive transport through the membranes and thus, enables prediction of bioavailability, intestinal absorption, and blood-brain barrier (BBB) penetration of drug (Kelder et al., 1999). The mean value of TPSA for the marketed drugs acting on CNS is 40.5 \AA^2 (range of $4.63\text{--}108 \text{ \AA}^2$) (Pajouhesh & Lenz, 2005). Molecules **9c** and **9f** have seven rotatable bonds each with TPSA respective values of 32.27 \AA^2 and 31.32 \AA^2 . In *In-silico* the oral absorption of drug is indicated by QPCaco-2 value. This QPCaco-2 explains the permeability through gut-blood barrier. Values for compound **9c** and **9f** are observed above 500 which forecast better oral absorption. Similarly, The oral bioavailability of test compounds are also supported by the human oral absorption percent (% HOA). The potential of compound to cross the blood-brain barrier is very well predicted by the Brain/

blood partition coefficient (QPlogBB), apparent MDCK cell permeability (QPPMDCK) and *n*-octanol–water partition coefficient (QPlogP_{o/w}). For the drugs which penetrate the BBB passively have the QPlogP_{o/w} values around 3.76. QPPMDCK value, which is considered as apparent MDCK cell permeability in nm/s, is considered to be a good imitate for the BBB. Any value above 25 for QPPMDCK is considered as good, and the test compounds under study have qualified this criterion. As the predicted CNS value is 1 for the test and reference compounds, these can be predicted as CNS active. The binding ability of test compound with human serum albumin is predicted by QPlogK_hsa value. The QPlogK_hsa values for the test molecules under study, **9c** and **9f**, are observed in the recommended range of values. #Star indicates the number of parameters with values that fall outside the 95% range of similar values for known drugs. A large #star value suggests that the molecule is less druglike in comparison to a molecule with few #star value. Zero value of #star for compounds **9c** and **9f** make them to be druglike. Further, a compound having a tertiary nitrogen-containing moiety in its structure is a common feature in many CNS active drugs which confers a good brain penetration (Pajouhesh & Lenz, 2005) which both of these compounds **9c** and **9f** have. Thus, compounds **9c** and **9f** are predicted to have a promising pharmacokinetics profile, which would augment their pharmacological potential.

Conclusion

Considering the heterogeneity and multifaceted nature of AD, it was contemplated to merge two different biologically active moieties, indole and quinoxaline in a single scaffold to design a potential anti-AD drug. By molecular hybridization approach, a combination of indole ring and the quinoxaline ring resulted in indoloquinoxaline scaffold. Incorporation of various substituents in the indoloquinoxaline scaffold resulted in a novel series of anti-AD agents demonstrating good in vitro cholinesterase inhibitory activity. Among the three classes of compounds which were synthesized, **9f** was identified as the most potent and selective BuChE inhibitor (IC₅₀ = 0.96 μM, selectivity index = 0.17) having a two-fold higher BuChE inhibitory activity compared to the commercially approved reference drug donepezil (IC₅₀ = 1.87 μM). Moreover, compound **9f** is also endowed with self-induced Aβ₁₋₄₂ aggregation inhibitory activity (51.24% inhibition at 100 μM concentration). This anti-Aβ aggregatory activity is likely to be due to the presence of a planar aromatic tetracyclic indoloquinoxaline scaffold and a piperidine ring side chain in its structure. These derivatives also possessed moderate antioxidant activity. Molecular modeling studies indicated significant interactions between compound **9f** and ChEs and Aβ₁₋₄₂ in their active sites. Compound **9f** showed good BBB permeation in PAMPA-BBB assay and favourable in silico ADME properties. Taken together, all these findings suggest compound **9f** to be a potential candidate for further development as a novel anti-AD drug.

Experimental section

General

All the required chemicals, reagents and solvents were procured from S. d. fine chemicals, Sigma-Aldrich, Spectrochem and Avra chemicals, and purified using general laboratory techniques whenever required. Precoated silica gel thin-layer chromatography (TLC), was used to monitor reaction progress and ultraviolet (UV) light (λ = 254 nm) or an iodine chamber was used for visualization. Flash column chromatography (Teledyne ISCO CombiFlash Rf system) with RediSep Rf columns were used for purification of compounds. All the reported yields are unoptimized. Melting points were determined using melting point apparatus (Veego) or by differential scanning calorimetry (DSC - Shimadzu DSC-60 instrument), and the reported melting points are uncorrected. Using Bruker ALPHA-T (Germany) FT-IR spectrophotometer all IR spectra were recorded. NMR (¹H and ¹³C) spectra were recorded on a Bruker Advance-II 400 MHz spectrometer either in CDCl₃ or DMSO-*d*₆ solvents and corresponding chemical shifts (δ) are expressed in parts per million (ppm) relative to the standard TMS, and the peak patterns are indicated as s (singlet), d (doublet), t (triplet), m (multiplet), and br (broad signal). Thermo Fisher mass spectrometer with an EI ion source was used to record the mass of compounds. For elemental analyses Thermo Fisher FLASH 2000 organic elemental analyzer was used. The elemental compositions of the compounds were within ±0.4% range of the calculated values.

Chemistry

6*h*-Indolo[2,3-*b*]quinoxaline (**3a**)

General procedure A

A mixture of isatin (**2a**) (1 g, 0.006 mol) and 1,2-diaminobenzene (0.734 g, 0.006 mol) in glacial acetic acid (10 mL) was taken into RBF and irradiated in microwave for about 10 min at 180 W. Progress of the reaction was monitored by TLC. After completion of the reaction, the reaction mixture was poured in ice-cold water and neutralized with a saturated sodium bicarbonate solution to pH 7. The solid so obtained was filtered, dried, and recrystallized to get compound **3a** as a yellow solid (0.37 g, 79%). m.p. 289.93 °C (DSC); IR (KBr, cm⁻¹): 3138, 2960, 2926, 1597, 1404, 744; ¹H NMR (CDCl₃): δ 11.94 (bs, 1H, -NH), 8.35–8.33 (d, 1H, ArH), 8.25–8.21 (m, 1H, ArH), 8.07–8.05 (m, 1H, ArH), 7.79–7.75 (m, 1H, ArH), 7.71–7.65 (m, 2H, ArH), 7.58–7.56 (d, 1H, ArH), 7.37–7.33 (m, 1H, ArH); MS (m/z): 220.10 (M + H)⁺.

Synthesis of 6-substituted 6*h*-indolo[2,3-*b*]quinoxaline derivatives (**3b-3l**)

Following the **General Procedure (A)**, 6-substituted 6*h*-indolo[2,3-*b*]quinoxaline derivatives **3b-3l** were synthesized by condensation of *N*₁-substituted isatins with 1,2-diaminobenzene. The obtained solids were recrystallized to yield the titled compounds.

6-Methyl-6H-indolo[2,3-b]quinoxaline (3b)

Pale yellow solid; yield 76%; m.p. 150–152 °C; IR (KBr, cm^{-1}): 3055, 2966, 1583, 1388, 1112, 748; ^1H NMR (CDCl_3): δ 8.39–8.37 (d, 1H, ArH), 8.26–8.23 (m, 1H, ArH), 8.12–8.10 (m, 1H, ArH), 7.82–7.75 (m, 2H, ArH), 7.73–7.69 (m, 2H, ArH), 7.43–7.39 (m, 1H, ArH), 3.96 (s, 3H, $-\text{CH}_3$); MS (m/z): 234.20 (M + H) $^+$.

6-Ethyl-6H-indolo[2,3-b]quinoxaline (3c)

Pale yellow solid; yield 75%; m.p. 136–138 °C; IR (KBr, cm^{-1}): 3055, 2970, 1608, 1585, 1409, 1116, 742; ^1H NMR (CDCl_3): δ 8.40–8.38 (d, 1H, ArH), 8.27–8.24 (m, 1H, ArH), 8.13–8.11 (m, 1H, ArH), 7.83–7.69 (m, 4H, ArH), 7.43–7.39 (m, 1H, ArH), 4.57–4.56 (m, 2H, $-\text{CH}_2$), 1.47–1.43 (t, 3H, $-\text{CH}_3$); ^{13}C NMR ($\text{DMSO}-d_6$): δ 145.08, 144.30, 140.41, 140.07, 139.05, 131.94, 129.53, 127.97, 126.54, 122.80, 121.45, 119.06, 110.78, 36.31, 13.88; MS (m/z): 248.20 (M + H) $^+$.

6-Isopropyl-6H-indolo[2,3-b]quinoxaline (3d)

Pale yellow solid; yield 70%; m.p. 144–146 °C; IR (KBr, cm^{-1}): 2985, 2968, 1608, 1579, 1382, 1234, 748; ^1H NMR (CDCl_3): δ 8.41–8.39 (d, 1H, ArH), 8.24–8.22 (m, 1H, ArH), 8.10–8.08 (m, 1H, ArH), 7.80–7.67 (m, 4H, ArH), 7.40–7.36 (m, 1H, ArH), 5.42–5.39 (m, 1H, $-\text{NCH}$), 1.78–1.77 (d, 6H, $-\text{CH}_3$); MS (m/z): 262.20 (M + H) $^+$.

6-Butyl-6H-indolo[2,3-b]quinoxaline (3e)

Pale yellow solid; yield 68%; m.p. 115–117 °C; IR (KBr, cm^{-1}): 3055, 2960, 2887, 1606, 1581, 1371, 1112, 746; ^1H NMR (CDCl_3): δ 8.39–8.37 (d, 1H, ArH), 8.26–8.24 (m, 1H, ArH), 8.11–8.09 (m, 1H, ArH), 7.80–7.67 (m, 4H, ArH), 7.41–7.37 (m, 1H, ArH), 4.53–4.49 (m, 2H, $-\text{NCH}_2$), 1.94–1.86 (m, 2H, $-\text{CH}_2$), 1.42–1.37 (m, 2H, $-\text{CH}_2$), 0.97–0.94 (t, 3H, $-\text{CH}_3$); ^{13}C -NMR (CDCl_3): 145.51, 144.73, 140.44, 139.93, 139.05, 131.95, 129.54, 128.03, 126.57, 122.75, 121.45, 118.98, 110.96, 41.20, 30.54, 20.19, 14.15; MS (m/z): 276.20 (M + H) $^+$.

6-Benzyl-6H-indolo[2,3-b]quinoxaline (3f)

Pale yellow solid; yield 74%; m.p. 172–174 °C; IR (KBr, cm^{-1}): 3084, 2980, 2960, 1581, 1408, 1197, 742; ^1H NMR (CDCl_3): δ 8.41–8.39 (d, 1H, ArH), 8.28–8.26 (m, 1H, ArH), 8.13–8.11 (m, 1H, ArH), 7.81–7.77 (m, 1H, ArH), 7.73–7.65 (m, 2H, ArH), 7.58–7.56 (d, 1H, ArH), 7.41–7.35 (m, 3H, ArH), 7.30–7.21 (m, 3H, ArH), 5.75 (s, 2H, $-\text{CH}_2-$); ^{13}C -NMR (CDCl_3): δ 145.66, 144.53, 140.49, 140.02, 139.35, 137.36, 132.00, 129.76, 129.62, 129.24, 128.03, 127.64, 126.85, 122.85, 121.86, 119.27, 111.12, 44.72; MS (m/z): 310.14 (M + H) $^+$.

6-(2-Bromobenzyl)-6H-indolo[2,3-b]quinoxaline (3g)

Pale yellow solid; yield 71%; m.p. 194–196 °C; IR (KBr, cm^{-1}): 3057, 2980, 1587, 1404, 1154, 756; ^1H NMR (CDCl_3): δ 8.45–8.43 (d, 1H, ArH), 8.29–8.27 (m, 1H, ArH), 8.08–8.06 (m, 1H, ArH), 7.80–7.66 (m, 4H, ArH), 7.46–7.41 (m, 2H, ArH), 7.22–7.18 (m, 1H, ArH), 7.15–7.11 (m, 1H, ArH), 6.73–6.71 (m, 1H, ArH), 5.76 (s, 2H, $-\text{CH}_2$); MS (m/z): 388.20 (M + H) $^+$.

6-(3-Fluorobenzyl)-6H-indolo[2,3-b]quinoxaline (3h)

Pale yellow solid; yield 76%; m.p. 137–140 °C; IR (KBr, cm^{-1}): 3062, 2980, 1587, 1408, 1253, 748; ^1H NMR (CDCl_3): δ 8.42–8.40 (d, 1H, ArH), 8.30–8.28 (m, 1H, ArH), 8.14–8.12 (m, 1H, ArH), 7.84–7.59 (m, 4H, ArH), 7.43–7.39 (m, 1H, ArH), 7.32–7.28 (m, 1H, ArH), 7.21–7.16 (m, 2H, ArH), 7.05–7.00 (m, 1H, ArH), 5.59 (s, 2H, $-\text{CH}_2$); MS (m/z): 328.20 (M + H) $^+$.

6-(3-Trifluoromethylbenzyl)-6H-indolo[2,3-b]quinoxaline (3i)

Pale yellow solid; yield 68%; m.p. 183–185 °C; IR (KBr, cm^{-1}): 3034, 2980, 1585, 1327, 1166, 750; ^1H NMR (CDCl_3): δ 8.42–8.40 (d, 1H, ArH), 8.29–8.27 (m, 1H, ArH), 8.12–8.09 (m, 1H, ArH), 7.82–7.78 (m, 1H, ArH), 7.75–7.67 (m, 2H, ArH), 7.62–7.54 (m, 5H, ArH), 7.43–7.39 (m, 1H, ArH), 5.85 (s, 2H, $-\text{CH}_2$); MS (m/z): 378.20 (M + H) $^+$.

6-(4-Cynobenzyl)-6H-indolo[2,3-b]quinoxaline (3j)

Pale yellow solid; yield 74%; m.p. 148–150 °C; IR (KBr, cm^{-1}): 2972, 2306, 1587, 1409, 1253, 750; ^1H NMR (CDCl_3): δ 8.40–8.38 (d, 1H, ArH), 8.27–8.25 (m, 1H, ArH), 8.12–8.10 (m, 1H, ArH), 7.80–7.76 (m, 1H, ArH), 7.73–7.66 (m, 2H, ArH), 7.59–7.57 (d, 1H, ArH), 7.41–7.37 (m, 1H, ArH) 7.32–7.27 (m, 1H, ArH), 7.17–7.14 (m, 2H, ArH), 7.01–6.97 (m, 1H, ArH), 5.74 (s, 2H, $-\text{CH}_2$); ^{13}C -NMR (CDCl_3): δ 145.62, 144.40, 140.44, 140.07, 139.42, 132.01, 131.33, 131.24, 129.70, 129.62, 128.06, 126.85, 123.62, 122.86, 121.93, 119.33, 114.99, 114.78, 114.69, 114.47, 111.17, 44.22.

6-(4-Methylbenzyl)-6H-indolo[2,3-b]quinoxaline (3k)

Pale yellow solid; yield 72%; m.p. 206–208 °C; IR (KBr, cm^{-1}): 3053, 2990, 1581, 1469, 1197, 742; ^1H NMR (CDCl_3): δ 8.40–8.38 (d, 1H, ArH), 8.28–8.26 (m, 1H, ArH), 8.13–8.11 (m, 1H, ArH), 7.81–7.79 (m, 1H, ArH), 7.74–7.66 (m, 2H, ArH), 7.61–7.59 (d, 1H, ArH), 7.41–7.37 (m, 1H, ArH), 7.26–7.24 (d, 2H, ArH), 7.09–7.07 (d, 2H, ArH), 5.70 (s, 2H, $-\text{CH}_2$), 2.24 (s, 3H, ArCH_3); MS (m/z): 324.15 (M + H) $^+$.

6-(4-Tert-Butylbenzyl)-6H-indolo[2,3-b]quinoxaline (3l)

Pale yellow solid; yield 77%; m.p. 164–166 °C; IR (KBr, cm^{-1}): 3057, 2964, 1585, 1406, 1114, 746; ^1H NMR (CDCl_3): δ 8.40–8.38 (d, 1H, ArH), 8.27–8.25 (d, 1H, ArH), 8.12–8.10 (d, 1H, ArH), 7.81–7.77 (m, 1H, ArH), 7.73–7.61 (m, 3H, ArH), 7.40–7.28 (m, 5H, ArH), 5.69 (s, 2H, $-\text{CH}_2$), 1.21 (s, 9H, $-\text{C}(\text{CH}_3)_3$); MS (m/z): 366.20 (M + H) $^+$.

Synthesis of 5-substituted 5H-indolo[2,3-b]quinoxaline derivatives (7a-7k)

Following the **General Procedure (A)**, 5-substituted 5H-indolo[2,3-b]quinoxaline derivatives **7a-7k** were synthesized by condensation of isatin (**2a**) with N_1 -substituted 1,2-diamines (**6a-6k**). The obtained solids were recrystallized to yield the titled compounds.

5-Benzyl-5H-indolo[2,3-b]quinoxaline (7a)

Pale yellow solid; yield 67%; m.p. 215–218 °C; IR (KBr, cm^{-1}): 3064, 2980, 2962, 1579, 1438, 1288, 746; ^1H NMR (CDCl_3): δ 8.29–8.27 (m, 1H, ArH), 8.24–8.22 (m, 1H, ArH), 7.90–7.88 (m, 1H, ArH), 7.76–7.72 (m, 1H, ArH), 7.68–7.64 (m, 1H, ArH), 7.61–7.56 (m, 2H, ArH), 7.35–7.25 (m, 6H, ArH), 6.14 (s, 2H, $-\text{CH}_2$); MS (m/z): 310.10 (M + H) $^+$.

5-(4-Methylbenzyl)-5H-indolo[2,3-b]quinoxaline (7b)

Pale yellow solid; yield 68%; m.p. 209–211 °C; IR (KBr, cm^{-1}): 2980, 2887, 1579, 1566, 1438, 1290, 754; ^1H NMR (CDCl_3): δ 8.28–8.26 (m, 1H, ArH), 8.24–8.22 (m, 1H, ArH), 7.90–7.88 (d, 1H, ArH), 7.75–7.71 (m, 1H, ArH), 7.68–7.64 (m, 1H, ArH), 7.61–7.55 (m, 2H, ArH), 7.32–7.28 (m, 1H, ArH), 7.25–7.23 (d, 2H, ArH), 7.11–7.09 (d, 2H, ArH), 6.08 (s, 2H, $-\text{CH}_2$), 2.24 (s, 3H, ArCH₃); MS (m/z): 324.20 (M + H) $^+$.

5-(2-Fluorobenzyl)-5H-indolo[2,3-b]quinoxaline (7c)

Pale yellow solid; yield 63%; m.p. 196–198 °C; IR (KBr, cm^{-1}): 3032, 2960, 1579, 1438, 1138, 748; ^1H NMR (CDCl_3): δ 8.28–8.21 (m, 2H, ArH), 7.92–7.90 (m, 1H, ArH), 7.76–7.72 (m, 1H, ArH), 7.68–7.64 (m, 1H, ArH), 7.61–7.56 (m, 2H, ArH), 7.45–7.42 (m, 2H, ArH), 7.32–7.28 (m, 1H, ArH), 7.10–7.06 (m, 2H, ArH), 6.11 (s, 2H, $-\text{CH}_2$); MS (m/z): 328.10 (M + H) $^+$.

5-(3-Fluorobenzyl)-5H-indolo[2,3-b]quinoxaline (7d)

Pale yellow solid; yield 59%; m.p. 202–204 °C; IR (KBr, cm^{-1}): 2980, 2889, 1579, 1438, 1138, 748; ^1H NMR (CDCl_3): δ 8.29–8.27 (m, 1H, ArH), 8.24–8.22 (m, 1H, ArH), 7.89–7.87 (m, 1H, ArH), 7.77–7.73 (m, 1H, ArH), 7.68–7.64 (m, 1H, ArH), 7.61–7.57 (m, 2H, ArH), 7.36–7.28 (m, 2H, ArH), 7.24–7.22 (d, 1H, ArH), 7.16–7.14 (d, 1H, ArH), 7.08–7.04 (m, 1H, ArH), 6.13 (s, 2H, $-\text{CH}_2$); MS (m/z): 328.10 (M + H) $^+$.

5-(3-Chlorobenzyl)-5H-indolo[2,3-b]quinoxaline (7e)

Pale yellow solid; yield 66%; m.p. 198–200 °C; IR (KBr, cm^{-1}): 3057, 2980, 1579, 1436, 1288, 746; ^1H NMR (CDCl_3): δ 8.30–8.28 (m, 1H, ArH), 8.24–8.22 (m, 1H, ArH), 7.89–7.87 (m, 1H, ArH), 7.77–7.75 (m, 1H, ArH), 7.66–7.59 (m, 1H, ArH), 7.61–7.59 (m, 2H, ArH), 7.49 (s, 1H, ArH), 7.32–7.25 (m, 4H, ArH), 6.13 (s, 2H, $-\text{CH}_2$); MS (m/z): 344.10 (M + H) $^+$.

5-(2-Methoxybenzyl)-5H-indolo[2,3-b]quinoxaline (7f)

Pale yellow solid; yield 53%; m.p. 218–220 °C; IR (KBr, cm^{-1}): 2980, 2972, 1577, 1429, 1246, 752; ^1H NMR (CDCl_3): δ 8.31–8.29 (m, 1H, ArH), 8.24–8.22 (m, 1H, ArH), 7.73–7.56 (m, 5H, ArH), 7.31–7.23 (m, 2H, ArH), 7.13–7.11 (m, 1H, ArH), 6.72–6.68 (m, 1H, ArH), 6.59–6.57 (m, 1H, ArH), 6.02 (s, 2H, $-\text{CH}_2$), 4.10 (s, 3H, $-\text{OCH}_3$); MS (m/z): 340.10 (M + H) $^+$.

5-(4-Methoxybenzyl)-5H-indolo[2,3-b]quinoxaline (7g)

Pale yellow solid; yield 58%; m.p. 216–218 °C; IR (KBr, cm^{-1}): 3051, 2968, 1579, 1438, 1247, 742; ^1H NMR (CDCl_3): δ 8.29–8.22 (m, 2H, ArH), 7.98–7.96 (m, 1H, ArH), 7.78–7.74 (m,

1H, ArH), 7.67–7.57 (m, 2H, ArH), 7.35–7.28 (m, 3H, ArH), 6.86–6.84 (m, 3H, ArH), 6.06 (s, 2H, $-\text{CH}_2$), 3.69 (s, 3H, $-\text{OCH}_3$); MS (m/z): 340.20 (M + H) $^+$.

5-(3,4-Dimethoxybenzyl)-5H-indolo[2,3-b]quinoxaline (7h)

Pale yellow solid; yield 59%; m.p. 224–226 °C; IR (KBr, cm^{-1}): 2970, 2902, 1579, 1438, 1259, 752; ^1H NMR (CDCl_3): δ 8.28–8.22 (m, 1H, ArH), 7.98–7.96 (m, 1H, ArH), 7.77–7.73 (m, 1H, ArH), 7.68–7.56 (m, 3H, ArH), 7.31–7.28 (m, 1H, ArH), 7.21–7.07 (m, 1H, ArH), 6.80–6.74 (m, 3H, ArH), 6.05 (s, 2H, $-\text{CH}_2$), 3.78 (s, 3H, $-\text{OCH}_3$), 3.76 (s, 3H, $-\text{OCH}_3$); ^{13}C -NMR (CDCl_3): δ 159.29, 153.45, 149.36, 147.04, 133.36, 130.95, 130.80, 128.30, 124.30, 123.08, 121.55, 119.60, 118.90, 116.13, 112.44, 112.07, 55.98, 48.56, 40.56; MS (m/z): 370.20 (M + H) $^+$.

5-Phenylethyl-5H-indolo[2,3-b]quinoxaline (7i)

Pale yellow solid; yield 68%; m.p. 184–186 °C; IR (KBr, cm^{-1}): 2980, 2885, 1564, 1454, 1244, 746; ^1H NMR (CDCl_3): δ 8.28–8.26 (m, 1H, ArH), 8.21–8.19 (m, 1H, ArH), 8.07–8.05 (m, 1H, ArH), 7.83–7.79 (m, 1H, ArH), 7.66–7.58 (m, 3H, ArH), 7.41–7.39 (m, 2H, ArH), 7.33–7.22 (m, 4H, ArH), 5.09–5.05 (m, 2H, ArCH₂), 3.27–3.23 (m, 2H, $-\text{NCH}_2$); ^{13}C -NMR (CDCl_3): δ 159.19, 153.08, 146.14, 136.30, 134.77, 133.25, 130.93, 130.89, 129.45, 129.00, 127.20, 124.17, 123.15, 122.93, 121.41, 118.91, 115.64, 46.67, 33.32; MS (m/z): 324.120 (M + H) $^+$.

5-(4-Chlorophenylethyl)-5H-indolo[2,3-b]quinoxaline (7j)

Pale yellow solid; yield 63%; m.p. 185–187 °C; IR (KBr, cm^{-1}): 2980, 2889, 1566, 1444, 1290, 752; ^1H NMR (CDCl_3): δ 8.26–8.24 (m, 1H, ArH), 8.20–8.18 (m, 1H, ArH), 8.01–7.99 (m, 1H, ArH), 7.81–7.77 (m, 1H, ArH), 7.64–7.56 (m, 3H, ArH), 7.41–7.39 (m, 2H, ArH), 7.32–7.25 (m, 3H, ArH), 5.07–5.03 (m, 2H, ArCH₂), 3.28–3.24 (m, 2H, $-\text{NCH}_2$); MS (m/z): 358.20 (M + H) $^+$.

5-(3,4-Dimethoxyphenylethyl)-5H-indolo[2,3-b]quinoxaline (7k)

Pale yellow solid; yield 57%; m.p. 159–160 °C; IR (KBr, cm^{-1}): 2980, 2972, 1564, 1460, 1136, 746; ^1H NMR (CDCl_3): δ 8.25–8.23 (m, 1H, ArH), 8.19–8.17 (m, 1H, ArH), 7.98–7.96 (m, 1H, ArH), 7.79–7.75 (m, 1H, ArH), 7.65–7.55 (m, 3H, ArH), 7.27–7.24 (m, 1H, ArH), 6.94 (s, 1H, ArH), 6.85–6.79 (m, 2H, ArH), 5.07–5.03 (m, 2H, ArCH₂), 3.76 (s, 3H, $-\text{OCH}_3$), 3.74 (s, 3H, $-\text{OCH}_3$), 3.21–3.17 (m, 2H, $-\text{NCH}_2$); MS (m/z): 384.20 (M + H) $^+$.

General procedure for the synthesis of 6-(bromoalkyl)-6H-indolo[2,3-b]quinoxaline (8a-8c)

To a stirred suspension of 6H-indolo [2,3-b]quinoxaline (**3a**) (2.39 g, 10 mmol) in THF (30 mL) was added sodium hydroxide (2.81 g, 50 mmol). The obtained solution was stirred for 30 min at 45 °C and dibromoalkane (50 mmol) was added. The reaction mixture was heated to reflux for 6 h, the reaction progress was monitored by TLC. After completion of the reaction, the reaction mixture was evaporated under reduced

pressure. The residue was dissolved in chloroform and washed with water. The collected organic layer was dried over sodium sulfate, filtered and evaporated to give a crude product which was purified by column chromatography.

6-(4-Bromobutyl)-6H-indolo[2,3-b]quinoxaline (8a)

Yellow solid; yield 85%; MS (m/z): 354.48 [M]⁺, 356.44 [M + 2]⁺

6-(5-Bromopentyl)-6H-indolo[2,3-b]quinoxaline (8b)

Yellow solid; yield 79%; MS (m/z): 368.49 [M]⁺, 370.46 [M + 2]⁺

6-(6-Bromohexyl)-6H-indolo[2,3-b]quinoxaline (8c)

Yellow solid; yield 79%; MS (m/z): 382.55 [M]⁺, 384.51 [M + 2]⁺

General procedure for the synthesis of 6-(aminoalkyl)-6H-indolo[2,3-b]quinoxaline (9a-9f)

To a solution of 6-(bromoalkyl)-6H-indolo[2,3-b]quinoxaline (**8a-8c**) (1 mmol) in THF (15 mL), piperidine or pyrrolidine (10 mmol) was added. The reaction mixture was refluxed under a nitrogen atmosphere. Progress of the reaction was monitored by TLC. After completion of the reaction, the reaction mixture was evaporated under reduced pressure and the residue was dissolved in 20 mL of water and extracted with chloroform (3 × 20 mL). The collected organic layer was again washed with water, dried over anhydrous magnesium sulfate, filtered and evaporated to give a crude product which was further purified by column chromatography.

6-(4-(Pyrrolidin-1-yl)butyl)-6H-indolo[2,3-b]quinoxaline (9a)

Pale yellow solid; yield 70%; m.p. 71–73 °C; IR (KBr, cm⁻¹): 3056, 2927, 2863, 2788, 1607, 1582, 1467, 1240, 751; ¹H NMR (CDCl₃): δ 8.48 (d, 1H, ArH), 8.29 (d, 1H, ArH), 8.12 (d, 1H, ArH), 7.77–7.65 (m, 3H, ArH), 7.50–7.48 (m, 1H, ArH), 7.39–7.36 (m, 1H, ArH), 4.54–4.51 (m, 2H, -NCH₂), 2.53–2.47 (m, 6H, -NCH₂), 2.03–1.99 (m, 2H, -NCH₂CH₂), 1.82–1.72 (m, 4H, -NCH₂CH₂), 1.68–1.64 (m, 2H, -NCH₂CH₂); MS (m/z): 345.3 [M + H]⁺.

6-(5-(Pyrrolidin-1-yl)pentyl)-6H-indolo[2,3-b]quinoxaline (9b)

Pale yellow solid; yield 67%; m.p. 101–103 °C; IR (KBr, cm⁻¹): 3056, 2927, 2851, 2758, 1607, 1579, 1463, 1118, 747; ¹H NMR (DMSO-*d*₆): δ 8.45 (d, 1H, ArH), 8.30–8.28 (m, 1H, ArH), 8.12–8.10 (m, 1H, ArH), 7.75–7.64 (m, 3H, ArH), 7.46–7.33 (m, 2H, ArH), 4.48–4.46 (m, 2H, -NCH₂), 2.41–2.37 (m, 6H, -NCH₂), 1.97–1.95 (m, 2H, -NCH₂CH₂), 1.65–1.57 (m, 6H, -NCH₂CH₂), 1.42–1.140 (m, 2H, -NCH₂CH₂CH₂); MS (m/z): 359.3 [M + H]⁺.

6-(6-(Pyrrolidin-1-yl)hexyl)-6H-indolo[2,3-b]quinoxaline (9c)

Pale yellow solid; yield 73%; m.p. 98–100 °C; IR (KBr, cm⁻¹): 3053, 2926, 2856, 2778, 1606, 1579, 1464, 1112, 751; ¹H NMR (DMSO-*d*₆): δ 8.49–8.46 (m, 1H, ArH), 8.30–8.28 (m, 1H, ArH), 8.14–8.12 (m, 1H, ArH), 7.76–7.66 (m, 3H, ArH), 7.46–7.35 (m, 2H, ArH), 4.48–4.45 (m, 2H, -NCH₂), 2.51–2.40 (m, 6H, -NCH₂), 1.97–1.95 (m, 2H, -NCH₂CH₂), 1.79–1.77 (m, 4H, -NCH₂CH₂), 1.54–1.52 (m, 2H, -NCH₂CH₂) 1.42–1.40 (m, 4H, -NCH₂CH₂CH₂CH₂); ¹³C-NMR (DMSO-*d*₆): 145.05, 144.20, 139.97, 139.47, 138.62, 131.41, 129.10, 129.01, 127.54, 126.05, 122.25, 120.94, 118.53, 110.51, 55.39, 53.47, 53.45, 26.55, 26.19, 25.53, 25.05, 22.94; MS (m/z): 373.3 [M + H]⁺.

6-(4-(Piperidin-1-yl)butyl)-6H-indolo[2,3-b]quinoxaline (9d)

Pale yellow solid; yield 70%; m.p. 92–94 °C; IR (KBr, cm⁻¹): 3056, 2926, 2860, 2782, 1607, 1580, 1467, 1237, 751; ¹H NMR (DMSO-*d*₆): δ 8.40 (d, 1H, ArH), 8.28 (dd, *J* = 8.4 Hz, 1.2 Hz, 1H, ArH), 8.13 (dd, *J* = 8.4 Hz, 1.2 Hz, 1H, ArH), 7.85–7.72 (m, 4H, ArH) 7.44–7.40 (m, 1H, ArH), 4.52–4.49 (m, 2H, -NCH₂), 2.52–2.34 (m, 6H, -NCH₂), 1.94–1.87 (m, 2H, -NCH₂CH₂), 1.63–1.60 (m, 4H, -NCH₂CH₂), 1.54–1.46 (m, 2H, -NCH₂CH₂CH₂), 1.38–1.31 (m, 2H, -NCH₂CH₂CH₂); MS (m/z): 359.3 [M + H]⁺.

6-(5-(Piperidin-1-yl)pentyl)-6H-indolo[2,3-b]quinoxaline (9e)

Pale yellow solid; yield 72%; m.p. 96–98 °C; IR (KBr, cm⁻¹): 3058, 2930, 2851, 2793, 1610, 1579, 1467, 1114, 766; ¹H NMR (DMSO-*d*₆): δ 8.50–8.45 (m, 1H, ArH), 8.34–8.27 (m, 1H, ArH), 8.14–8.12 (m, 1H, ArH), 7.75–7.66 (m, 3H, ArH), 7.44–7.36 (m, 2H, ArH), 4.45–4.48 (m, 2H, -NCH₂), 2.52–2.27 (m, 6H, -NCH₂), 1.94–1.87 (m, 2H, -NCH₂CH₂), 1.63–1.60 (m, 4H, -NCH₂CH₂), 1.42–1.39 (m, 4H, indole NCH₂CH₂CH₂); MS (m/z): 373.3 [M + H]⁺.

6-(6-(Piperidin-1-yl)hexyl)-6H-indolo[2,3-b]quinoxaline (9f)

Pale yellow solid; yield 69%; m.p. 99–101 °C; IR (KBr, cm⁻¹): 3053, 2927, 2852, 2762, 1607, 1579, 1463, 1112, 753; ¹H NMR (DMSO-*d*₆): δ 8.51–8.47 (m, 1H, ArH), 8.33–8.29 (m, 1H, ArH), 8.16–8.13 (m, 1H, ArH), 7.80–7.67 (m, 3H, ArH), 7.50–7.38 (m, 2H, ArH), 4.52–4.47 (m, 2H, -NCH₂), 2.40–2.24 (m, 6H, -NCH₂), 1.99–1.94 (m, 2H, -NCH₂CH₂), 1.70–1.42 (m, 6H, -NCH₂CH₂, 4H, -NCH₂CH₂CH₂, 2H, -NCH₂CH₂CH₂CH₂); ¹³C-NMR (DMSO-*d*₆): 145.05, 144.25, 139.98, 139.47, 138.62, 131.41, 129.10, 128.99, 127.55, 126.05, 122.25, 120.93, 118.53, 110.50, 58.35, 53.90, 27.74, 26.58, 26.19, 25.98, 25.53, 25.37, 24.00; MS (m/z): 387.3 [M + H]⁺.

General procedure for the synthesis of 1-(6-(6H-indolo[2,3-b]quinoxalin-6-yl)hexyl)alkylamide (10a, 10b)

To a stirred suspension of sodium hydride (1 mmol) in dry THF (15 mL), 2-pyrrolidinone or 2-piperidinone (1 mmol) was added at 0 °C under a blanket of dry nitrogen. The reaction mixture was stirred for 30 min. 6-(6-Bromohexyl)-6H-

indolo[2,3-*b*]quinoxaline (**8c**) dissolved in a minimum amount of dry THF was added into the reaction mixture at 0 °C, and then brought slowly up to room temperature and left to stir overnight. After completion of the reaction, the reaction mixture was evaporated under reduced pressure and the residue was dissolved in 20 mL of water and extracted with chloroform (3 × 20 mL). The collected organic layer was again washed with water, dried over anhydrous magnesium sulfate, filtered and evaporated to give a crude product which was further purified by column chromatography.

1-(6-(6*h*-Indolo[2,3-*b*]quinoxalin-6-yl)hexyl)pyrrolidin-2-one (**10a**)

Pale yellow solid; yield 52%; m.p. 102–104 °C; IR (KBr, cm⁻¹): 3053, 2927, 2852, 2762, 1607, 1579, 1463, 1112, 753; ¹H NMR (DMSO-*d*₆): δ 8.50 (d, 1H, *ArH*), 8.31 (dd, *J* = 8.4 Hz, 1.2 Hz, 1H, *ArH*), 8.15 (dd, *J* = 8.4 Hz, 1.2 Hz, 1H, *ArH*) 7.80–7.68 (m, 3H, *ArH*), 7.50–7.48 (m, 1H, *ArH*), 7.40–7.38 (m, 1H, *ArH*), 4.52–4.49 (m, 2H, -NCH₂), 3.33–3.30 (m, 2H, -CONCH₂), 3.27–3.23 (m, 2H, -CONCH₂) 1.99–1.94 (m, 4H, -COCH₂CH₂), 1.50–1.38 (m, 2H, -CONCH₂CH₂, 4H, -NCH₂CH₂CH₂CH₂); MS (m/z): 387.3 [M + H]⁺.

1-(6-(6*h*-Indolo[2,3-*b*]quinoxalin-6-yl)hexyl)piperidin-2-one (**10b**)

Pale yellow solid; yield 58%; m.p. 63–65 °C; IR (KBr, cm⁻¹): 3057, 2937, 2858, 1632, 1578, 1464, 1118, 761; ¹H NMR (DMSO-*d*₆): δ 8.40 (d, 1H, *ArH*), 8.28 (dd, *J* = 8.4 Hz, 1.2 Hz, 1H, *ArH*), 8.13 (dd, *J* = 8.4 Hz, 1.2 Hz, 1H, *ArH*) 7.85–7.73 (m, 4H, *ArH*), 7.44–7.42 (m, 1H, *ArH*), 4.52–4.49 (m, 2H, -NCH₂), 3.19–3.12 (m, 4H, -CONCH₂), 2.15–2.12 (m, 2H, -COCH₂), 1.91–1.87 (m, 2H, -COCH₂CH₂), 1.64–1.62 (m, 4H, -CONCH₂CH₂), 1.40–1.28 (m, 2H, -NCH₂CH₂, 4H, -NCH₂CH₂CH₂CH₂); ¹³C-NMR (DMSO-*d*₆): 167.96, 145.03, 144.24, 139.97, 139.46, 138.61, 131.41, 129.09, 128.99, 127.55, 126.05, 122.25, 120.93, 118.53, 110.49, 60.39, 46.97, 45.97, 31.93, 27.76, 26.39, 26.13, 26.01, 22.73, 20.97; MS (m/z): 401.3 [M + H]⁺.

Biology

Inhibition studies on AChE and BuChE

The ability of the test compounds to inhibit ChEs was assessed using Ellman's method as detailed in our earlier report (Patel et al., 2019, Patel et al., 2020).

Antioxidant activity [1,1-Diphenyl-2-picrylhydrazyl (DPPH) radical scavenging activity]

The antioxidant potential of the compounds was assessed using spectrophotometric DPPH assay as described earlier (Patel et al., 2019, Patel et al., 2020).

Self-induced Aβ₁₋₄₂ aggregation inhibition study

The potency, to inhibit the self-mediated Aβ₁₋₄₂ aggregation, of indolo[2,3-*b*]quinoxaline derivatives was evaluated by a thioflavin T (ThT)-based fluorescence assay reported previously (Li et al., 2013; Patel et al., 2020).

In vitro blood-brain barrier permeation assay

The PAMPA assay was carried out to determine the BBB permeation of the most active compound **9f** as described previously (Patel et al., 2019, Patel et al., 2020).

Computational studies

Docking studies of compound **9f** and **9c** with ChEs

Docking studies of the active compounds with ChEs were carried out with the Glide (2018) module of Schrodinger Suite. 3D structures of the ligand molecules were constructed by the Build module within Maestro, and low energy conformation was searched for the ligand/compound under consideration at physiological pH condition by using the OPLS3e force field within the Ligprep (2018) module of Schrödinger. PDB structures of AChE (PDB code: 2CKM, 1B41) and of BuChE (PDB code: 4BDS) were retrieved from the Protein Data Bank (RCSB) (Protein Data Bank, 2019) and prepared for docking using the protein preparation wizard. Using extra-precision (XP) mode, molecular docking calculations were carried out within the active sites of the receptor structures. The followed docking protocol was validated by comparing the interactions of donepezil within the active site (Cheung et al., 2012).

Docking studies of compound **9f** with Aβ₁₋₄₂

AutoDock4.2 (Morris et al., 2009; Sanner, 1999) was used to perform this docking analysis. Aβ₁₋₄₂ peptide structure was retrieved from RCSB site (PDB Code: 1IYT). It was cleaned and prepared for docking analysis within AutoDock tool. The blind docking was performed for compound **9f**. Grid was generated over the entire protein structure, and compound **9f** was allowed to dock with the entire amino acid sequence to understand the most possible/stable interactions between the **9f** and the peptide sequence. For this study, 10 docking experiments were run using the Lamarckian genetic algorithm. The maximum number of energy evaluations of 25 million was applied for every docking experiment.

Molecular dynamics simulation studies

To determine the ligand receptor stability over a period of time, molecular dynamics study was performed between the most active compound **9f** and AChE and BuChE protein structures by using GROMACS 2018.1 software (Abraham et al., 2018). The best docked pose of the ligand with the respective receptor was taken as the starting point for simulation. To determine the complex stability CHARMM36 all-atom force field (Huang et al., 2017) was used and ligand-

receptor parameters were derived in GROMACS. For this purpose, the ligand topology was generated using the CGenFF server (Vanommeslaeghe et al., 2010; Yu et al., 2012) and ligand-receptor complexes were built. These receptor-ligand complex systems were solvated using SPC water model (Mark & Nilsson, 2001). To neutralize the total charge on the individual system, in AChE-9f complex 6 NA were added, in BuChE-9f complex 7 CL ions were added and in A β_{1-42} -9f complex 2 NA were added to the system. All the complexes were first energy minimized using steepest descent method (Bixon & Lifson, 1967) followed by two sequential equilibration simulations using canonical (NVT) and isobaric-isothermic (NPT) ensemble for 100 picoseconds (ps) each. Using the NPT ensemble the production MD simulation was performed and the long-range electrostatic interactions were identified by using particle mesh Ewald (PME) method (Darden et al., 1993). The molecular dynamics simulation was carried out for 10 ns at 300 K temperature and 1 bar pressure using the GROMACS 2018.1 simulation package.

In silico prediction of physicochemical and pharmacokinetics parameters

The *in silico* pharmacokinetic and physicochemical properties were determined using QikProp module (Schrodinger LLC, New York) (QikProp, 2018). All the ligand structures were generated using Maestro Build module and energy minimization was carried out using OPLS3e force field at physiological pH conditions using LigPrep module of Schrödinger and were used for Qik-Prop properties calculation.

Acknowledgement

The authors thank Dr. Kapil Juvale, SPPSPTM, NMIMS University, Mumbai for providing SpectramMax iD3 multi-mode microplate reader to perform A β_{1-42} aggregation study.

Author contributions

MRY conceptualized the whole study. AMK, DVP, and NRP performed synthesis and collected data. PST and KBP contributed reagents, materials and helped in synthesis and data collection. AMK performed computational studies. KVP drafted the biological evaluation studies. AS and KBP performed the biological studies and collected data. NKP helped in synthesis and data interpretation. AMK, DVP, and NRP wrote the manuscript. MRY comprehended and approved the final version of the manuscript.

Disclosure statement

There are no conflicts of interest to disclose.

Funding

Mange Ram Yadav acknowledges the University Grant Commission (UGC), New Delhi, for providing UGC-BSR Faculty Fellowship [No. F.18-1/2011(BSR)]. Dushyant V. Patel is thankful to the DST-INSPIRE, New Delhi for awarding Research Fellowship (IF-150660). Nirav R. Patel acknowledges the UGC, New Delhi, for awarding Senior Research Fellowship [F. No. 25-1/2014-15(BSR)/7-129/2007/(BSR)].

References

- Abraham, M. J., van der Spoel, D., Lindahl, E., & Hess, B. (2018). GROMACS user manual version.
- Avula, S., Komsani, J., Koppireddi, S., Yadla, R., Kanugula, A., & Kotamraju, S. (2012). Synthesis and cytotoxicity of novel 6H-indolo [2, 3-b] quinoxaline derivatives. *Medicinal Chemistry Research*, 22(8), 3712–3718.
- Bartus, R. T., Dean, R. R., Beer, B., & Lippa, A. S. (1982). The cholinergic hypothesis of geriatric memory dysfunction. *Science (New York, N.Y.)*, 217(4558), 408–414. <https://doi.org/10.1126/science.7046051>
- Bixon, M., & Lifson, S. (1967). Potential functions and conformations in cycloalkanes. *Tetrahedron*, 23, 769–784.
- Bonda, D. J., Wang, X., Perry, G., Nunomura, A., Tabaton, M., Zhu, X., & Smith, M. A. (2010). Oxidative stress in Alzheimer disease: A possibility for prevention. *Neuropharmacology*, 59(4–5), 290–294. <https://doi.org/10.1016/j.neuropharm.2010.04.005>
- Brunhofer, G., Fallarero, A., Karlsson, D., Batista-Gonzalez, A., Shinde, P., Gopi Mohan, C., & Vuorela, P. (2012). Exploration of natural compounds as sources of new bifunctional scaffolds targeting cholinesterases and beta amyloid aggregation: The case of chelerythrine. *Bioorganic & Medicinal Chemistry*, 20(22), 6669–6679. <https://doi.org/10.1016/j.bmc.2012.09.040>
- Cavalli, A., Bolognesi, M. L., Minarini, A., Rosini, M., Tumiatti, V., Recanatini, M., & Melchiorre, C. (2008). Multi-target-directed ligands to combat neurodegenerative diseases. *Journal of Medicinal Chemistry*, 51(3), 347–372. <https://doi.org/10.1021/jm7009364>
- Cheignon, C., Tomas, M., Bonnefont-Rousselot, D., Faller, P., Hureau, C., & Collin, F. (2018). Oxidative stress and the amyloid beta peptide in Alzheimer's disease. *Redox Biology*, 14, 450–464. <https://doi.org/10.1016/j.redox.2017.10.014>
- Cheung, J., Rudolph, M. J., Burshteyn, F., Cassidy, M. S., Gary, E. N., Love, J., Franklin, M. C., & Height, J. J. (2012). Structures of human acetylcholinesterase in complex with pharmacologically important ligands. *Journal of Medicinal Chemistry*, 55(22), 10282–10286. <https://doi.org/10.1021/jm300871x>
- Darden, T., York, D., & Pedersen, L. (1993). Particle mesh Ewald: An N -log(N) method for Ewald sums in large systems. *Journal of Chemical Physics*, 98(12), 10089–10092. <https://doi.org/10.1063/1.464397>
- Di, L., Kerns, E. H., Fan, K., McConnell, O. J., & Carter, G. T. (2003). High throughput artificial membrane permeability assay for blood-brain barrier. *European Journal of Medicinal Chemistry*, 38(3), 223–232.
- Di, L., Kerns, E. H., Bezar, I. F., Petusky, S. L., & Huang, Y. (2009). Comparison of blood-brain barrier permeability assays: in situ brain perfusion, MDR1-MDCKII and PAMPA-BBB. *Journal of Pharmaceutical Sciences*, 98, 1980–1991.
- Dighe, S. N., Deora, G. S., De la Mora, E., Nachon, F., Chan, S., Parat, M. O., Brazzolotto, X., & Ross, B. P. (2016). Discovery and structure-activity relationships of a highly selective butyrylcholinesterase inhibitor by structure-based virtual screening. *Journal of Medicinal Chemistry*, 59, 7683–7689.
- Glide. (2018). *Glide*. Schrodinger, LLC.
- Greenough, M. A., Camakaris, J., & Bush, A. I. (2013). Metal dyshomeostasis and oxidative stress in Alzheimer's disease. *Neurochemistry International*, 62(5), 540–555. [Database] <https://doi.org/10.1016/j.neuint.2012.08.014>
- Greig, N. H., Lahiri, D. K., & Sambamurti, K. (2002). Butyrylcholinesterase: An important new target in Alzheimer's Disease therapy. *International Psychogeriatrics*, 14(S1), 77–91. <https://doi.org/10.1017/S1041610203008676>
- Greig, N. H., Utsuki, T., Ingram, D. K., Wang, Y., Pepeu, G., Scali, C., Yu, Q.-S., Mamczarz, J., Holloway, H. W., & Giordano, T. (2005). Selective butyrylcholinesterase inhibition elevates brain acetylcholine, augments learning and lowers Alzheimer -amyloid peptide in rodent. *Proceedings of the National Academy of Sciences*, 102(47), 17213–17218.
- Gu, Z., Li, Y., Ma, S., Li, S., Zhou, G., Ding, S., Zhang, J., Wang, S., & Zhou, C. (2017). Synthesis, cytotoxic evaluation and DNA binding study of 9-fluoro-6H-indolo[2,3-b]quinoxaline derivatives. *RSC Advances*, 7(66), 41869–41879. <https://doi.org/10.1039/C7RA08138C>
- Hardy, J. A., & Higgins, G. A. (1992). Alzheimer's disease: The amyloid cascade hypothesis. *Science*, 256(5054), 184–186.

- Hartmann, J., Kiewert, C., Duysen, E. G., Lockridge, O., Greig, N. H., & Klein, J. (2007). Excessive hippocampal acetylcholine levels in acetylcholinesterase-deficient mice are moderated by butyrylcholinesterase activity. *Journal of Neurochemistry*, *100*(5), 1421–1429. <https://doi.org/10.1111/j.1471-4159.2006.04347.x>
- Huang, J., Rauscher, S., Nawrocki, G., Ran, T., Feig, M., de Groot, B. L., Grubmüller, H., & MacKerell Jr, A. D. (2017). CHARMM36m: An improved force field for folded and intrinsically disordered proteins. *Nature Methods*, *14*(1), 71–73. <https://doi.org/10.1038/nmeth.4067>
- Kanhed, A. M., Sinha, A., Machhi, J., Tripathi, A., Parikh, Z. S., Pillai, P. P., Giridhar, R., & Yadav, M. R. (2015). Discovery of isoalloxazine derivatives as a new class of potential anti-Alzheimer agents and their synthesis. *Bioorganic Chemistry*, *61*, 7–12.
- Kelder, J., Grootenhuys, P. D., Bayada, D. M., Delbressine, L. P., & Ploemen, J.-P. (1999). Polar molecular surface as a dominating determinant for oral absorption and brain penetration of drugs. *Pharmaceutical Research*, *16*(10), 1514–1519. <https://doi.org/10.1023/A:1015040217741>
- Lane, C. A., Hardy, J., & Schott, J. M. (2018). Alzheimer's disease. *European Journal of Neurology*, *25*(1), 59–70. <https://doi.org/10.1111/ene.13439>
- Lane, R. M., Potkin, S. G., & Enz, A. (2006). Targeting acetylcholinesterase and butyrylcholinesterase in dementia. *The International Journal of Neuropsychopharmacology*, *9*, 101–124.
- Li, S.-Y., Wang, X.-B., Xie, S.-S., Jiang, N., Wang, K. D., Yao, H.-Q., Sun, H.-B., & Kong, L.-Y. (2013). Multifunctional tacrine-flavonoid hybrids with cholinergic, β -amyloid-reducing, and metal chelating properties for the treatment of Alzheimer's disease. *European Journal of Medicinal Chemistry*, *69*, 632–646. <https://doi.org/10.1016/j.ejmech.2013.09.024>
- Ligprep. (2018). *Ligprep*. Schrödinger, LLC.
- Lipinski, C. A., Lombardo, F., Dominy, B. W., & Feeney, P. J. (1997). Experimental and computational approaches to estimate solubility and permeability in drug discovery and development settings. *Advanced Drug Delivery Reviews*, *23*(1–3), 3–25. [Database] [https://doi.org/10.1016/S0169-409X\(96\)00423-1](https://doi.org/10.1016/S0169-409X(96)00423-1)
- Lobo, V., Patil, A., Phatak, A., & Chandra, N. (2010). Free radicals, antioxidants and functional foods: Impact on human health. *Pharmacognosy Reviews*, *4*(8), 118–126. <https://doi.org/10.4103/0973-7847.70902>
- López-Iglesias, B., Pérez, C., Morales-García, J. A., Alonso-Gil, S., Pérez-Castillo, A., Romero, A., López, M. G., Villarroya, M., Conde, S., & Rodríguez-Franco, M. I. (2014). New melatonin-N,N-dibenzyl(N-methyl)amine hybrids: Potent neurogenic agents with antioxidant, cholinergic, and neuroprotective properties as innovative drugs for Alzheimer's disease. *Journal of Medicinal Chemistry*, *57*(9), 3773–3785. <https://doi.org/10.1021/jm5000613>
- Maccioni, R. B., Farias, G., Morales, I., & Navarrete, L. (2010). The revitalized tau hypothesis on Alzheimer's disease. *Archives of Medical Research*, *41*(3), 226–231. <https://doi.org/10.1016/j.arcmed.2010.03.007>
- Mark, P., & Nilsson, L. (2001). Structure and dynamics of the TIP3P, SPC, and SPC/E water models at 298 K. *Journal of Physical Chemistry A*, *43*, 9954–9960.
- McEneny-King, A., Osman, W., Edginton, A. N., & Rao, P. P. N. (2017). Cytochrome P450 binding studies of novel tacrine derivatives: Predicting the risk of hepatotoxicity. *Bioorganic & Medicinal Chemistry Letters*, *27*(11), 2443–2449. <https://doi.org/10.1016/j.bmcl.2017.04.006>
- Morris, G. M., Huey, R., Lindstrom, W., Sanner, M. F., Belew, R. K., Goodsell, D. S., & Olson, A. J. (2009). AutoDock4 and AutoDockTools4: Automated docking with selective receptor flexibility. *Journal of Computational Chemistry*, *30*(16), 2785–2791.
- O'Brien, R. J., & Wong, P. C. (2011). Amyloid precursor protein processing and Alzheimer's disease. *Annual Review of Neuroscience*, *34*, 185–204.
- Pachon-Angona, I., Refouvet, B., Andrys, R., Martin, H., Luzet, V., Iriepa, I., Moraleda, I., Diez-Iriepa, D., Oset-Gasque, M. J., Marco-Contelles, J., Musilek, K., & Ismaili, L. (2019). Donepezil + chromone + melatonin hybrids as promising agents for Alzheimer's disease therapy. *Journal of Enzyme Inhibition and Medicinal Chemistry*, *34*, 479–489.
- Pajouhesh, H., & Lenz, G. R. (2005). Medicinal chemical properties of successful central nervous system drugs. *NeuroRx: The Journal of the American Society for Experimental Neurotherapeutics*, *2*(4), 541–553. <https://doi.org/10.1602/neuroRx.2.4.541>
- Patel, D. V., Patel, N. R., Kanhed, A. M., Patel, S. P., Sinha, A., Kansara, D. D., Mecwan, A. R., Patel, S. B., Upadhyay, P. N., Patel, K. B., Shah, D. B., Prajapati, N. K., Murumkar, P. R., Patel, K. V., & Yadav, M. R. (2019). Novel multitarget directed triazinoindole derivatives as anti-alzheimer agents. *ACS Chemical Neuroscience*, *10*, 3635–3661.
- Patel, D. V., Patel, N. R., Kanhed, A. M., Teli, D. M., Patel, K. B., Joshi, P. D., Patel, S. P., Gandhi, P. M., Chaudhary, B. N., Prajapati, N. K., Patel, K. V., & Yadav, M. R. (2020). Novel carbazole-stilbene hybrids as multifunctional anti-Alzheimer agents. *Bioorganic Chemistry*, *101*, 103977.
- Patterson, C. (2018). *Alzheimer's Disease International*. ADI.
- Pohanka, M. (2011). Cholinesterases, a target of pharmacology and toxicology. *Biomedical Papers of the Medical Faculty of Palacky University in Olomouc*, 155.
- Protein Data Bank. (2019). Retrieved August 9, 2019, from www.rcsb.org/pdb/home/home.do.
- QikProp. (2018). *QikProp*. Schrödinger, LLC.
- Ramos, E., Palomino-Antolin, A., Bartolini, M., Iriepa, I., Moraleda, I., Diez-Iriepa, D., Samadi, A., Cortina, C. V., Chioua, M., Egea, J., Romero, A., & Marco-Contelles, J. (2019). QuinoxalineTacrines QT78, a Cholinesterase inhibitor as a potential ligand for Alzheimer's Disease therapy. *Molecules (Basel, Switzerland)*, *24*(8), 1503.
- Rodríguez-Franco, M. I., Fernández-Bachiller, M. I., Pérez, C., Hernández-Ledesma, B., & Bartolomé, B. (2006). Novel tacrine-melatonin hybrids as dual-acting drugs for Alzheimer disease, with improved acetylcholinesterase inhibitory and antioxidant properties. *Journal of Medicinal Chemistry*, *49*(2), 459–462. <https://doi.org/10.1021/jm050746d>
- Sanner, M. F. (1999). Python: a programming language for software integration and development. *Journal of Molecular Graphics and Modelling*, *17*, 57–61.
- Scheltens, P., Blennow, K., Breteler, M. M., de Strooper, B., Frisoni, G. B., Salloway, S., & Van der Flier, W. M. (2016). Alzheimer's disease. *Lancet (London, England)*, *388*(10043), 505–517.
- Selkoe, D. J. (2003). Folding proteins in fatal ways. *Nature*, *426*, 900.
- Shidore, M., Machhi, J., Shingala, K., Murumkar, P., Sharma, M. K., Agrawal, N., Tripathi, A., Parikh, Z., Pillai, P., & Yadav, M. R. (2016). Benzylpiperidine-linked diarylthiazoles as potential anti-Alzheimer's agents: Synthesis and biological evaluation. *Journal of Medicinal Chemistry*, *59*, 5823–5846.
- Sinha, A., Tamboli, R. S., Seth, B., Kanhed, A. M., Tiwari, S. K., Agarwal, S., Nair, S., Giridhar, R., Chaturvedi, R. K., & Yadav, M. R. (2015). Neuroprotective role of novel triazine derivatives by activating Wnt/ β catenin signaling pathway in rodent models of Alzheimer's Disease. *Molecular Neurobiology*, *52*(1), 638–652.
- Talesa, V. N. (2001). Acetylcholinesterase in Alzheimer's disease. *Mechanisms of Ageing and Development*, *122*(16), 1961–1969. [https://doi.org/10.1016/S0047-6374\(01\)00309-8](https://doi.org/10.1016/S0047-6374(01)00309-8)
- Uttara, B., Singh, A. V., Zamboni, P., & Mahajan, R. (2009). Oxidative stress and neurodegenerative diseases: A review of upstream and downstream antioxidant therapeutic options. *Current Neuropharmacology*, *7*(1), 65–74. [Database] <https://doi.org/10.2174/157015909787602823>
- Vanommeslaeghe, K., Hatcher, E., Acharya, C., Kundu, S., Zhong, S., Shim, J., Darian, E., Guvench, O., Lopes, P., Vorobyov, I., & MacKerell Jr, A. D. (2010). CHARMM general force field: A force field for drug-like molecules compatible with the CHARMM all-atom additive biological force fields. *Journal of Computational Chemistry*, *31*, 671–690.
- Veber, D. F., Johnson, S. R., Cheng, H.-Y., Smith, B. R., Ward, K. W., & Kopple, K. D. (2002). Molecular properties that influence the oral bioavailability of drug candidates. *Journal of Medicinal Chemistry*, *45*(12), 2615–2623. <https://doi.org/10.1021/jm020017n>
- Yanovsky, I., Finkin-Groner, E., Zaikin, A., Lerman, L., Shalom, H., Zeeli, S., Weill, T., Ginsburg, I., Nudelman, A., & Weinstock, M. (2012). Carbamate derivatives of indolines as cholinesterase inhibitors and antioxidants for the treatment of Alzheimer's disease. *Journal of Medicinal Chemistry*, *55*(23), 10700–10715. <https://doi.org/10.1021/jm301411g>
- Yu, W., He, X., Vanommeslaeghe, K., & MacKerell Jr, A. D. (2012). Extension of the CHARMM general force field to sulfonyl-containing compounds and its utility in biomolecular simulations. *Journal of Computational Chemistry*, *33*, 2451–2468.
- Zhao, Y., & Zhao, B. (2013). Oxidative stress and the pathogenesis of Alzheimer's disease. *Oxidative Medicine and Cellular Longevity*, *2013*, 1–10.